ANL-6764
Reactor Technology
(TID-4500, 21st Ed.)
AEC Research and
Development Report

ARGONNE NATIONAL LABORATORY
9700 South Cass Avenue
Argonne, Illinois 60440

REACTOR DEVELOPMENT PROGRAM PROGRESS REPORT

July 1963

Albert V. Crewe, Laboratory Director

Division	Director
Chemical Engineering	R. C. Vogel
Idaho	M. Novick
Metallurgy	F. G. Foote
Reactor Engineering	L. J. Koch
Reactor Physics	R. Avery
Remote Control	R. C. Goertz

Report coordinated by
R. M. Adams and A. Glassner

Issued August 15, 1963

Operated by The University of Chicago
under
Contract W-31-109-eng-38
with the
U. S. Atomic Energy Commission

DISCLAIMER

FOREWORD

The Reactor Development Program Progress Report, issued monthly, is intended to be a means of reporting those items of significant technical progress which have occurred in both the specific reactor projects and the general engineering research and development programs. The report is organized in a way which, it is hoped, gives the clearest, most logical over-all view of progress. The budget classification is followed only in broad outline, and no attempt is made to report separately on each sub-activity number. Further, since the intent is to report only items of significant progress, not all activities are reported each month. In order to issue this report as soon as possible after the end of the month editorial work must necessarily be limited. Also, since this is an informal progress report, the results and data presented should be understood to be preliminary and subject to change unless otherwise stated.

The issuance of these reports is not intended to constitute publication in any sense of the word. Final results either will be submitted for publication in regular professional journals or will be published in the form of ANL topical reports.

The last six reports issued in this series are:

January 1963	ANL-6683
February 1963	ANL-6698
March 1963	ANL-6705
April 1963	ANL-6717
May 1963	ANL-6739
June 1963	ANL-6764

TABLE OF CONTENTS

TABLE OF CONTENTS

TABLE OF CONTENTS

I. BOILING WATER REACTORS

A. BORAX-V

1. Operation

Room-temperature, zero-power experiments on the central superheater core CSH-1 were completed this month, and zero-power experiments at pressures and temperatures up to operating conditions (600 psig, 489°F) were started.

In preparation for measurements of the superheater flooding time and reactivity addition rate, the detachable bottom nozzles of four central superheater fuel assemblies were welded on and assemblies were leak-tested. Weld leaks in the assemblies were repaired, and special in-core instrumentation for flooding-time measurements was installed. Considerable time was spent in trouble-shooting ion chamber and counter circuits to assure good period measurements.

A check was made of the boric acid concentration required in the reactor water to shut the reactor down at room temperature with all control rods completely withdrawn. The measured curve of available excess reactivity vs. boric acid concentration, extrapolated to the just-critical point, indicates a value of about 12.3 g H_3BO_3 per gal H_2O. With a concentration of 12.95 g H_3BO_3 per gal H_2O, the core CSH-1 was determined to be subcritical.

The reactivity worth of a central superheater fuel assembly vs. water in core position 35 was measured to be 0.84% at room temperature. This compares to a calculated value of 1.0% reported in ANL-6302.[1]

Measurements of the effect of the neutron source on the critical positions of the control rod, and period measurements at low powers, indicated that a source drive would not be required for the zero-power experiments at operating temperatures. Critical experiment measurements made at reactor water levels of 2 ft, 4 ft, and 6 ft above the core indicate a negligible reactivity effect from these level changes.

2. Determination of the Reactivity Addition Rate on Flooding the Superheater

One of the unique potential hazards of a small, integral, boiling-nuclear superheating reactor such as BORAX-V is accidental or inadvertent flooding of the superheater during operation. On a core with the size and composition of BORAX-V, superheater flooding yields a positive reactivity addition. Two modes of superheater flooding are possible: (1) by opening a

---

[1] Design and Hazards Summary Report, BORAX-V, ANL-6302.

superheater flood valve and flooding from below; and (2) by raising the level of the reactor water and flooding over the top of the inlet superheater fuel assembly risers.

To add reactivity by flooding the superheater from below during operation requires the lifting of a switch guard on the controls to the solenoid-tripped flood valve, or the removal of a padlock on the remote operator for the manual flood valve. The "flood-valve-open" scram interlocks would have to be bypassed. To prevent an accident even if these precautions failed, a flow-restricting orifice has been installed in the superheater flood line to slow the flooding time.

Flooding the superheater from above is potentially more hazardous because of a possible higher flooding rate. To add reactivity by raising the reactor water level rapidly and flooding over the top of the inlet superheater fuel assembly risers would require maloperation of the feedwater pumps, ignoring the high-reactor-water-level alarm, and failure of two independent high-reactor-water-level scram circuits. To lengthen the flooding time, the riser on one of the six inlet superheater fuel assemblies is 2 in. shorter than the remainder. The postulated sequence in flooding from above is as follows: Rising reactor water first floods over the short riser inlet superheater fuel assembly, flows down through this assembly, and fills the interpass plenum and parallel-connected lower superheated steam main before it begins to flood the remaining eleven assemblies from below. Before the flooding level reaches the top of the core, the rising reactor water level reaches the top of the other five standard inlet assembly risers, floods down through these assemblies, and speeds up the remaining bottom flooding of the six outlet assemblies.

a. Measurements. Because of the potential reactor hazard involved in measuring the reactivity addition rate of superheater flooding dynamically while critical, and because of the doubtful feasibility of direct subcritical dynamic measurements, the experiments were performed in two stages: First, the reactivity worth of the flooded central superheater was measured statically by critical experiments; and then the rate of flooding was measured with the reactor shut down. The results of these two experiments were then correlated to give reactivity addition rates. The reactivity measurements were made with the central control rod completely withdrawn. Both reactivity and flooding-time measurements were made at atmospheric pressure and temperatures of 79-83°F.

In the static reactivity measurements, the sequence of flooding from below was simulated at five different superheater water levels covering the core height, and also at normal reactor water level. To simulate the top flooding sequence, the reactivity measurements were made with the short riser inlet superheater fuel assembly (C-7) and interpass plenums flooded, and measurements were made with the flooding level in the remaining eleven assemblies at the base of the core (3.0 ft), 6 in. above the base

(3.5 ft), at the core midplane (4.0 ft), 18 in. above the core base (4.5 ft), at the core top (5.0 ft), and completely flooded at the normal reactor water level of 11.3 ft.

The time required to flood the central superheater was measured, both for the case when flooding occurred from below using the flood-and-drain system, and for the case of flooding from above in the event the reactor water level was increased. Three superheater assemblies (the short riser inlet assembly (C-7), a standard inlet assembly, and an outlet assembly) were each instrumented with two Teflon-insulated wires running axially in coolant channels. One wire in each assembly had uninsulated sensing points at the bottom, midpoint, and top of the fuel region; and the other wire had uninsulated sensing points at the $\frac{1}{4}$ and $\frac{3}{4}$ points. These wires were connected to a 6.3 v ac power supply through a 0.5 or 1 megohm resistor. The return circuit was through the fuel element and water. The ac signal developed across the resistor was rectified and recorded on an oscillograph. Water covering the sensing points produced steps in the signal level recorded. Some difficulty was experienced in the use of the instrumentation in the flooding-from-above tests, but repeated runs gave data which could be interpreted satisfactorily.

b. Results. The total central superheater flooding reactivity worth at room temperature with the central control rod withdrawn was +1.1%.[2] The time measured for flooding the reactor from below was 30-32 sec, which is very close to the calculated value. The maximum reactivity addition rate from opening the solenoid-trip flood valve and flooding from below was 0.03% per second.

The results of flooding the central superheater over the top are shown in Figure 1 for feedwater addition rates of 150 and 375 gpm. At time zero, the water hits the top of the fuel in the short inlet assembly, C-7. The maximum possible reactivity addition rate associated with running two feed pumps at a flow of 375 gpm was measured at 0.2% per second.

At these feedwater addition rates, the fueled region of the eleven remaining superheater fuel assemblies was flooded in about 5 sec, which was a greater time than was calculated. The major reason for the discrepancy was the effect of air bubbles rising through the falling column of water in the short inlet superheater fuel assembly riser.

If it is assumed that the effect of steam bubbles rising through the falling column of water is the same as for air bubbles, the flooding time under 489°F, 600 psig, zero-power operating conditions should be 5-10% less than at room temperature, due to changes in the density and viscosity

---

[2]Reactor Development Program Progress Report, June, 1963, ANL-6749.

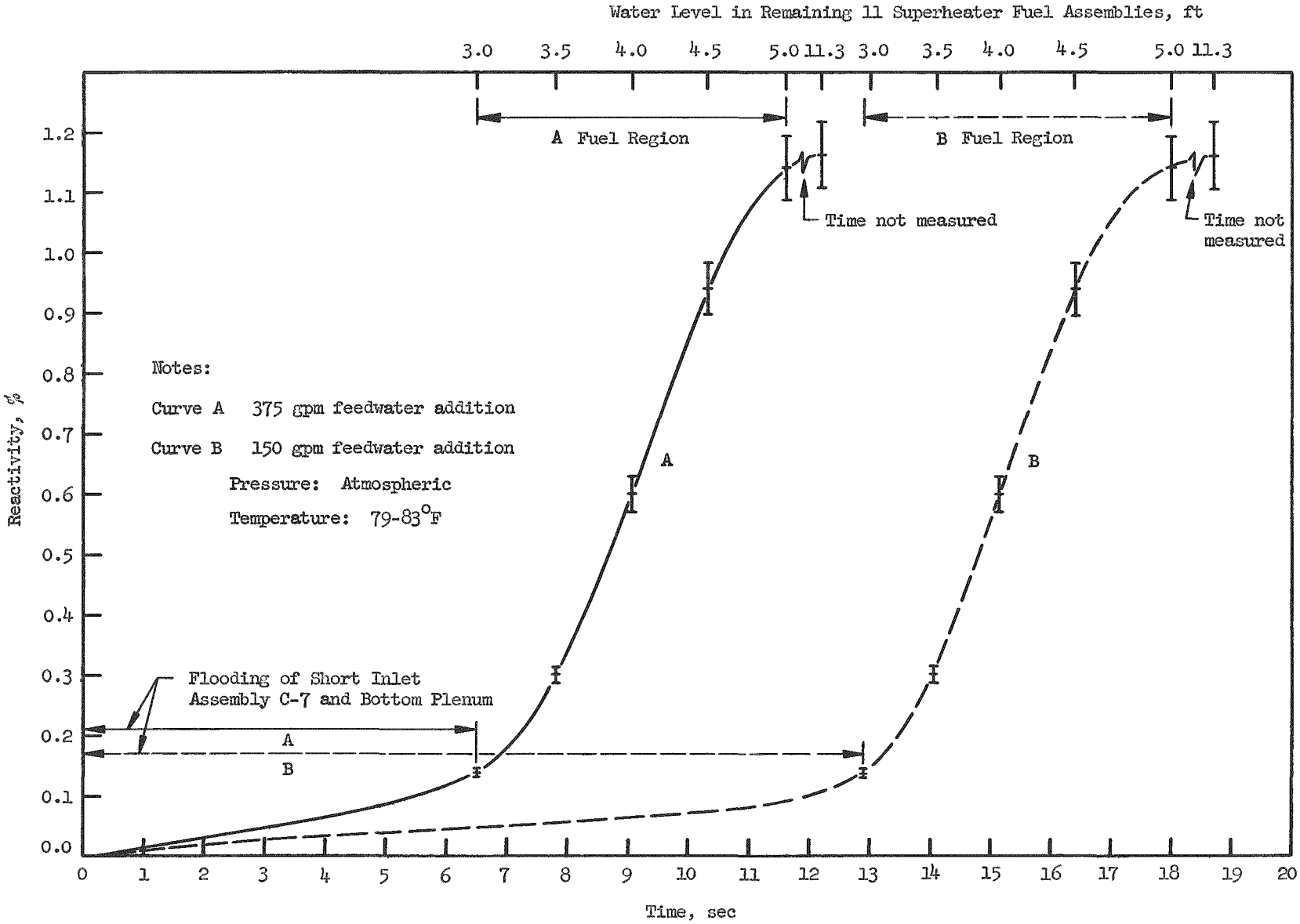

Figure 1. Reactivity vs. Time - Flooding Central Superheater from Top - Core CSH-1 - BORAX-V

of the water. At power conditions when the superheater fuel plates are at high temperature, flooding would be considerably retarded by steam generation and expulsion of the flooding water.

3. Analysis of Previous Experimental Data

Data reduction and analysis of flux-wire irradiations made last month in the central superheater core CSH-1 have yielded preliminary information on ability to control the power split between boiler and superheater. Several axial and radial flux traverses were made with chopped gold flux wires, with the central control rod above, below, and with the banked eight remaining control rods. Figure 2 illustrates the effect of the various control rod configurations on the diagonal radial neutron flux distribution at a plane 6 in. above the bottom of the core, with no boric acid in the reactor water, and at room temperature. As can be seen, the power split at this elevation is affected substantially by inserting the central control rod, No. 1, below the 8-control-rod bank, but very little by withdrawing rod No. 1 above the bank. The effect of flooding the central superheater with all control rods approximately banked may also be noted. Cadmium ratios were measured with gold flux wires in the core, at room temperature, with no boric acid. The ratios were for the central part of a superheater fuel assembly in a location symmetrical to core position 54 and gave a value of 1.4. A comparative value in a boiling fuel assembly in a location symmetrical to core position 63 was 2.5.

To study the effect on the disadvantage factors of different water-fuel ratios obtained by various flow rod configurations in a boiling core or boiler of an integral boiling-superheating core, PDQ cell problems have been prepared and are being run. Boiling assemblies containing 0, 4, 5, 6, 8, 12 and 16 flow rods are being considered. Results of the zero and 4-flow-rod problems have been received.

4. Water Chemistry

Monitoring of reactor water for various water chemistry parameters continued throughout the month. Early in the month, boric acid was removed from the reactor water by draining and filling, followed by a cleanup by intermittent operation of the reactor water demineralizer system. Boric acid concentration was reduced from a value of 12.95 g H_3BO_3 per gal H_2O to 0.1 ppm.

Checks on the gross specific gamma activity of the reactor water revealed no detectable activity. However, the suspended solids filtered out of the reactor water had a fairly high gamma activity varying from 4,540 to 8,690 cpm/mg. The concentrations of suspended solids in the reactor water remained low during the zero-power, room-temperature operation, ranging from 0.07 to 0.20 ppm of ignited oxides.

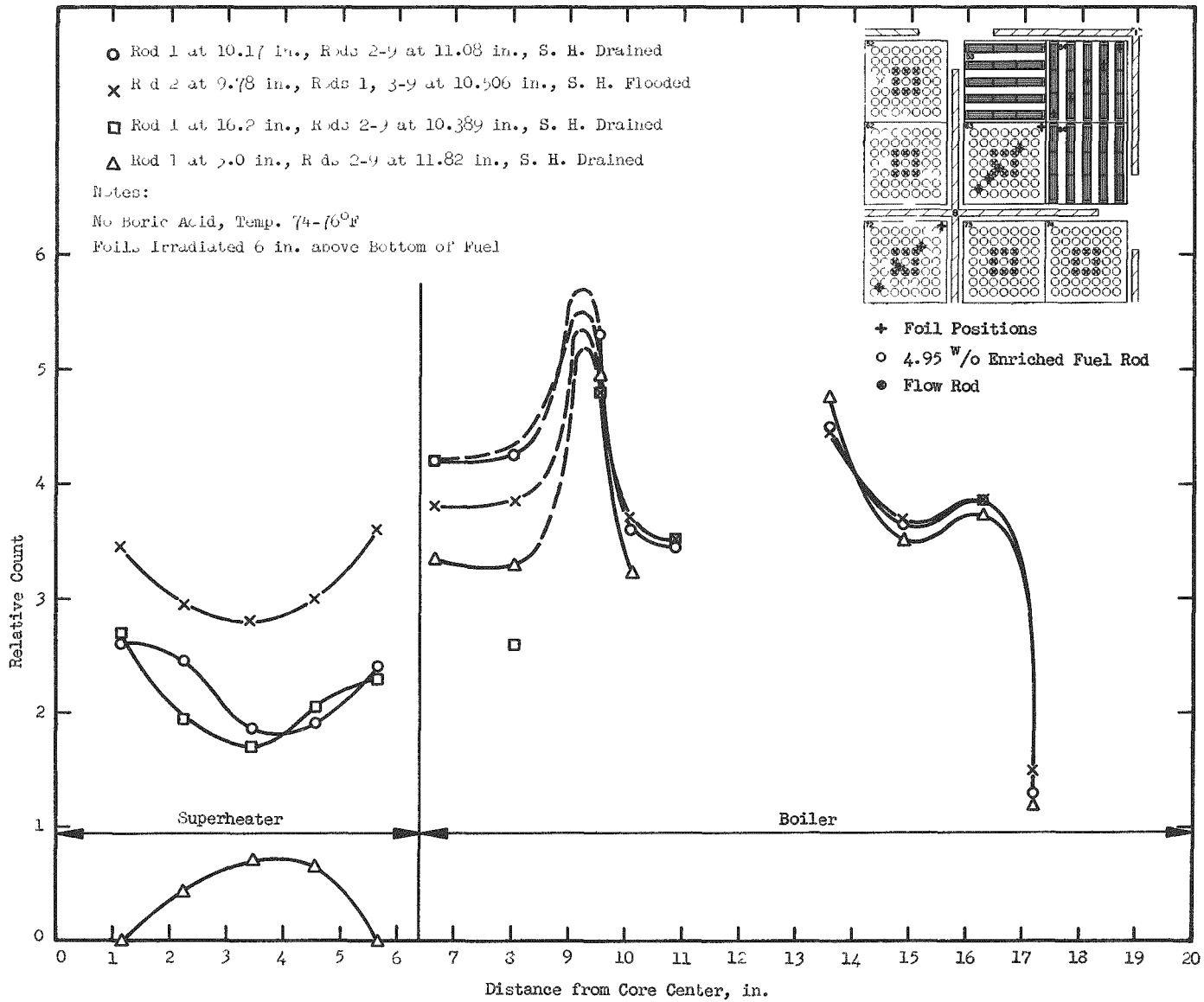

Figure 2. Radial Flux Distributions - Central Superheater Core CSH-1 - BORAX-V

Two samples analyzed radiochemically specifically for cesium isotopes showed no Cs and thus no detectable fission products.

5. Modifications and Maintenance

Additional interlocks, scrams, and orifices have been installed to provide increased protection against improper flooding or cooling of the superheater. A second high-reactor-water-level scram was installed as backup for the existing scram circuit. A second low-steam-flow scram was installed as backup for the present scram circuit.

The orifice installed to reduce the superheater flooding rate when flooding from below was relocated so that it will reduce the flooding time on both opening of a flood valve and inadvertent opening of the pressure equalizing valve. Inadvertent opening of this equalizing valve could cause condensate collected in the lower superheat main to be forced into the superheater. The size of the pressure-breakdown orifice in the superheater drain line was reduced to limit the steam flow through this line to 2,000 lb/hr. Inadvertent opening of the superheater drain valve will not bypass enough steam to cause overheating in the superheater.

New turbine-type flowmeter pickup coils, utilizing seal-welded cans, have been installed on instrumented boiling fuel assembly I-1. The assembly is being autoclaved to check for coil leaks and to dry out all instrument leads.

Instrumented superheater fuel assembly C-16 was brazed to seal the entrance steam thermocouples into their penetrations. Upon final cleanup and a negative air leak test, the assembly was placed in the autoclave, seals were leak-tested, and all thermocouples were intercalibrated at temperatures up to 490°F. One fuel plate thermocouple was found to have failed at the hot junction; resistance readings indicated one conductor broke free from the junction. The remainder of the couples performed satisfactorily.

Upon removal from the autoclave, after approximately 10 hours at temperatures between 200 and 490°F, the assembly was filled with water and all metal joints were checked for leaks. Several weld joints, as well as the thermocouple braze, were found to leak. A corresponding test on a standard superheater assembly also showed up faulty welds. A leak repair procedure on all superheater fuel assemblies is now being developed.

II. LIQUID METAL COOLED REACTORS

A. General Fast Reactor Physics

1. ZPR-VI

Approval for the operation of ZPR-VI was received on July 16, 1963. Loading of fuel into the facility commenced the same day and criticality of Assembly No. 1 was reached on July 23. The first loading is an all-metal assembly having a U^{238}/U^{235} ratio of about 7. It is expected that the initial measurements, such as Rossi alpha, fission ratios, material replacement coefficients, and control rod calibrations, will take several months to perform.

2. ZPR-III

Experiments were continued this month on Assembly 43, a two-zone mockup of a 4,000-liter power breeder reactor.

a. Central Reactivity Coefficients. Central reactivity worths were measured for Ta and three fissile samples. These results are listed in Table I. Additional measurements of nonfissile samples will be performed later.

Table I. Central Reactivity Coefficients

Material	Mass (kg)	Worth (Ih ± .5)	Reactivity Coefficient (Ih/kg)
Enriched U^{235}	0.2684	+15.2	56.6 ± 1.8
Enriched Pu^{239}	0.186	+14.7	79.3 ± 2.7
Enriched U^{233}	0.221	+22.4	101.1 ± 2.3
Tantalum	0.262	- 5.2	-19.8 ± 1.9

b. Doppler Effect. An experiment was designed to measure the neutron Doppler effect, or broadening of the resonance with increasing temperature. The technique employed is to measure the reactivity effect of two nearly identical samples in symmetrical locations in the central region. The samples in this experiment consist of about 2.2 kg of depleted uranium oxide. The reactivity difference is measured first with both samples cold, and then with one of the samples hot. During operation, the samples were driven in and out of the reactor and a series of measurements performed to eliminate the effects of reactor temperature drift.

The first measurement was made with sample No. 1 heated to an average temperature of about 520°C. The total reactivity difference between the hot and cold interchanges was measured as -0.40 Ih. Then, the second sample was heated and the difference between the hot and cold interchanges was again measured as -0.40 Ih. Since Sample No. 2 was located vertically below No. 1, this was taken to mean that there were no reactivity effects due to slumping or sagging of the elements. In general, the accuracy of all of the measurements in the Doppler series of experiments is limited by the effects of reactor temperature drift. The estimated value of uncertainty is about ±0.03 Ih The measurements are in good agreement with the value of -0.425 Ih determined from preliminary calculations. However, neither the experimental nor calculated value is final; and the results are given here only to show the order of magnitude of the Doppler effect.

The next step in the experiment was to load a half-inch-thick layer of natural boron carbide around the sample to be heated. The boron absorbs low energy neutrons and, hence, reduces the Doppler effect. The calculated hot-minus-cold difference was -0.07 Ih, and the measured value was also -0.07 Ih. It is again stressed that these are preliminary values and that calculational and experimental results are being analyzed further.

All the above measurements were made with a loading designed to minimize the Dancoff correction; i.e., interaction of the U^{238} in the Doppler sample with that in the core. This was accomplished by moving all of the uranium and steel in the drawers immediately surrounding the elements to the far side of the drawer. This left an environment around the samples consisting principally of sodium Next, the Dancoff correction was maximized by moving all the uranium in the surrounding drawers as close as possible to the Doppler samples, with the resulting measured hot-cold interchange of -0.37 Ih. Again, this is not final and is given only to indicate that the correction is small compared to measured Doppler effect.

Additional experiments are being planned

c. Miscellaneous. During a routine inspection, it was discovered that one plate of plutonium fuel plates had increased considerably in thickness. Its original jacketed dimensions were 1 in x 2 in. x $\frac{1}{8}$ in., and it contained 30 grams of plutonium as an alloy with 1 w/o aluminum. The metal had received a flash coating of nickel and was jacketed with stainless steel .012 in. thick.

At the time of inspection it was found that the thickness had increased to approximately $\frac{3}{8}$ in and the formerly flat face surfaces had become convex In spite of the drastic change in dimensions of the piece, no alpha activity was detected on its surface, on the inside of the storage pot, or on the surface of pieces which were stored with it This would

indicate that no failure of the jacket has occurred and attests to the integrity and the dependability of these fuel plates for use in experimental loadings in ZPR-III. This plate has been returned to Lemont, where it will be analyzed and the cause of the failure determined.

B. General Fast Reactor Fuel Development

1. Fast Reactor Fuel Jacket Development

Of the alloys mentioned in the June Progress Report (ANL-6749, p. 14), the Nb-3 w/o Mo-9 w/o Ti alloy was broken down at 850°C, annealed, and cold rolled to $\frac{1}{32}$ in. sheet stock. Hot rolling of the Nb-9 w/o Ti-8 w/o V, V-35 w/o Nb and Nb-20 w/o V alloys has not been successful to date. These alloys have now been recast and will be rolled at higher temperatures. The alloy Zr-29 w/o V-16 w/o Ti has been successfully hot worked but was damaged beyond use during the cold working and annealing process. This alloy is also being recast.

A 1.27 cm (0.5 in.) diameter fully recrystallized round of Nb-10 w/o Ti-5 w/o Zr (D-36) was cold rolled to 0.076 cm (0.030 in.) thick sheet for sodium corrosion coupons.

Studies for extrusion of duplex tubing have started. Two extrusions of duplex bars have been made to evaluate bond quality. One billet consisted of a V bar in a jacket of Type 304 stainless steel. The second billet consisted of a V bar with a 0.003 cm (0.0012 in.) thick Ni-plate in a jacket of Type 304 stainless steel. Both billets were cleaned and assembled in an inert atmosphere. Extrusion at 1200°C through a 1.0 cm (0.391 in.) diameter die (6.5 1 reduction ratio) was easily accomplished. X-ray examination showed no defects. Ultrasonic and metallographic examination of bond quality is in progress.

2. Corrosion of Fuel-Cladding Materials for Sodium Cooled Reactors

Four specimens of niobium alloys have been exposed to flowing sodium (.15 meters/sec) for 330 hours at 650°C. The oxygen content of the sodium was analyzed at 140 ppm. Zirconium turnings were used as an oxygen getter during exposure of the test samples. All of the specimens were given a vacuum-anneal stress-relief treatment. The results are summarized in Table II.

The Nb-1 w/o Zr and Nb-5 w/o Zr samples had non-adherent oxides, while the Nb-39 w/o V-1 w/o Ti exhibited an adherent oxide at the oxide-metal interface. The edges of the Nb-5 w/o Zr samples were split open in a laminar manner. The Nb-5 w/o Mo sample showed an "eroded" surface pattern of random channels. Surface laps were present

which extended above the surface of the sample resulting in apparent increase in thickness as noted in Table II. The laps may have been present as a result of fabrication and subsequently opened up during exposure to the liquid metal.

Table II. Weight Loss of Niobium Alloys Exposed to Flowing Sodium

Sample	Weight Loss, mg/cm^2*	Change in Thickness,* mm
Nb-1 w/o Zr	62.2	-13.66×10^{-2}
Nb-5 w/o Zr	37.35	$- 4.24 \times 10^{-2}$
Nb-5 w/o Mo	28.75	$+ 2.34 \times 10^{-2}$
Nb-39 w/o V-1 w/o Ti	22.70	$- 2.86 \times 10^{-2}$

*As removed from test and cleaned of sodium with alcohol and water and ultrasonically cleaned to remove non-adherent oxide.

3. Lithium Corrosion Studies at Elevated Temperatures

Apparatus and procedures are being developed for handling liquid lithium without chemical contamination. This preliminary work is being done in temporary facilities until suitable corrosion test apparatus may be obtained and assembled.

4. High Temperature Metal Fuels

The trend in the Fast Reactor Program is toward higher temperatures in the fuel. The compound, $(UPu)Fe_2$, appears to offer promise for operation in the 700°C to 900°C range. An alloy, U-17.4 w/o Pu-39 w/o Fe, was injection cast and removed from the Vycor molds successfully. About 7 w/o Fe in excess of the stoichiometric 32 w/o was added for ductility. The liquidus of this alloy was 1200°C ± 10°C; the solidus was 1090°C ± 10°C. These values were determined by thermal analysis. No definite break at 910°C was obtained even though there was an excess of 7 w/o Fe.

C. EBR-I, Mark IV

Transfer function measurements were completed at high inlet temperature (230°C), full coolant flow (960 gpm), and 960 kw.

The uranium outer blanket was then installed in place of the lead blanket for the purpose of irradiating foils of U^{235}, U^{238}, and Pu^{239}, in a simulated fuel rod thimble in the center of the reactor. The irradiation,

in connection with breeding gain measurements by radiochemical analysis, was performed in one hour at about 10 kw.

At the completion of the foil irradiation, the reactor was reloaded for power operation. A slight interference between the outer blanket and the reactor safety plug was encountered during the installation of the blanket. This was traced to a loosening of the transfer carrier mounting bolts. The situation has been corrected, and operation is normal.

D. EBR-II

1. Reactor Plant

The temporary plug for the M-1 primary pump nozzle was installed. After heating the bulk sodium to 550°F, circulation through the reactor was started using primary pump M-2. (See June Monthly Progress Report, ANL-6749, for a pump removal description.) The faulty primary pump, M-1, was disassembled and inspected to determine the cause of failure. The middle labyrinth seal and the pump shaft at the labyrinth elevation were found to be galled. A dimensional check revealed that the labyrinth was cocked with respect to the shaft center line due to the tilt of the bottom flange of the shield plug.

The pump shaft bowed principally due to high temperature caused by its rubbing on the aluminum-bronze labyrinth bushing. It is presumed that the situation became progressively worse as increasing temperature caused the bushing to expand inward due to the constraint offered by its relatively cool mounting support. This resulted in severe galling of the shaft and damage to the bushing.

The shield plug bottom flange is being remachined, and a new pump shaft and a new labyrinth bushing are being made by the manufacturer.

The M-2 pump was operated continuously at various speeds for five days to check its performance and provide initial circulation for the sodium filtering run. Several filters were then removed and examined after vacuum distillation of the sodium in the filters. Very small (less than a gram) amounts of carbonaceous particles and metal particles were found in each of the filters examined. A portion of the debris found in the filters is suspected to have been due to incomplete cleaning of the filters prior to initial installation in the reactor. The replacement filters were examined thoroughly before insertion into the reactor to insure their cleanliness prior to the second filter run.

The permanent argon system for the fuel unloading machine was installed, checked, and put into operation during the month. After approximately two weeks of operation, the turbocompressor for the argon system

was stopped due to failure of parts of the impeller Examination revealed that the failure was due to cracking of the casting which forms the hub of the impeller. New parts have been ordered to replace those damaged.

During the fuel handling operation for removal of the filter elements, the No. 2 reactor vessel cover locking mechanism jammed. This was the same difficulty as encountered on the No. 3 cover lock and reported previously in ANL-6705, March 1963, and ANL-6717, April 1963. A new bearing was installed, as was done on the No. 3 cover lock. At the same time, as a precautionary measure, this modification was also performed on the No. 1 cover lock.

On July 14, both instrument thimble cooling turbocompressors developed bearing trouble. The nuclear instruments were removed from their thimbles in the primary tank, with the exception of one which was blocked by parts for the M-1 pump removal equipment (temporary external cooling was provided for this instrument). After removal of the instruments, the turbocompressors were shut down and the bearings replaced. A vendor's representative was not able to determine the reason for the bearing failure, other than the possibility that the bearings themselves were faulty.

On July 24 during the fuel handling operations with filter elements, the large rotating shield plug became difficult to rotate. Although the exact nature of the difficulty has not been established, it has been determined that the difficulty is related to temperature distribution in the plug and/or rotating seal. Freedom of rotation can be achieved by altering the temperature distributions. Detailed investigation is continuing to determine the cause and to establish corrective procedures.

2. Sodium Boiler Plant

Activities during the month largely involved preparations for a proposed leak test of the EBR-II steam generator, using tritium as a tracer. The method of the proposed test was described in the Progress Report for June, ANL-6749.

At the beginning of this reporting period, tests were in progress to determine the ability of the liquid nitrogen-cooled cold trap to collect water vapor from the nitrogen sweep gas injected into the secondary sodium system. Three attempts to collect moisture from the evacuated sodium system in late June had been unsuccessful. Therefore, to test the trap performance, small amounts of water were introduced into the nitrogen sweep gas stream at the gas injection point. The results indicated that a recovery efficiency of 50% of the injected water could be realized within a reasonable sampling time.

Failure of the large stainless steel Dewar flask used for immersion of the cold trap in liquid nitrogen brought an end to cold-trapping runs on July 1. Pending procurement of a replacement Dewar flask and continuation of testing prerequisite to the tritium leak test, the secondary sodium system was filled with dry argon on July 3. The argon was admitted to the system through a "molecular sieve" dessicant column to insure a very low moisture content.

The argon in the system was monitored at regular intervals for water vapor and hydrogen content. Between 0730 on July 4 and 1600 on July 10, the dew point of the argon increased from approximately -85°F to approximately -52°F. Analyzed hydrogen concentrations, although somewhat erratic, increased from approximately 47 ppm, soon after filling of the system with argon, to approximately 445 ppm by 1600 on July 10.

While the sodium system was pressurized with argon, the evacuation system was modified to permit evacuation of the sodium system through the two vent lines which run from the evaporator sodium inlet headers to the surge tank. These vent lines have been disconnected from the surge tank. Previously, the evacuation system had been connected directly to the surge tank and there was an attendant possibility that the major portion of the nitrogen sweep gas might flow through the secondary pump directly to the surge tank, bypassing the steam generator. With evacuation from the sodium headers, all sweep gas must pass through the steam generator.

Between July 10 and 12, while the evacuation system was being reconnected, the sodium system contained argon at atmospheric pressure. The system was open to the atmosphere at times during this period.

The sodium system was repressurized with argon on July 12 and remained thus until July 15. Samples of system argon from the surge tank and from the yard piping (at the nitrogen injection point) taken about 1000 on July 15 showed, respectively, dew points of +10°F and +12°F and hydrogen contents of 835 and 825 ppm. The increases were probably due in large part to ingress of atmospheric moisture while the system was open during installation of the modified evacuation system.

Evacuation of the sodium system was started at 1700 on July 15. Several tests for determining the apparent atmospheric air inleakage rate were conducted between the start of evacuation and the start of nitrogen sweep gas flow at 0100 on July 18 Results of the inleakage tests were considered satisfactory. The pressure of the system stabilized at about 50 microns.

During the period July 18 through 20, a series of cold-trapping runs were made to determine the activity background in the sodium system. The first four runs were made with the copper oxide recombiner heated and with nitrogen purge gas flow. The next four runs were made with purge gas flow but with the recombiner unheated. The results of these runs are tabulated in Table III.

Table III. Tritium Activity Determined by Cold-Trapping

Run No.	Date and Time Conditions	Water Added	Water Trapped	Tritium Activity
1	7/18/63, 0935-1235. Recombiner on, nitrogen purge on.	25 ml (0940-1030)	8 ± 1 ml	Combined with samples 2 and 3.
2	7/18/63, 1500-1800. Same conditions as "1."	None	4.4 ± 1 ml	Combined with samples 1 and 3.
3	7/18/63, 1950-2230. Same conditions as "1."	None	2.5 ± 1 ml	Combined with samples 1 and 2 3×10^{-4} μc/ml
4	2354, 7/18/63 to 0830, 7/19/63. Same conditions as "1."	None	5 ± 1 ml	No analysis.
5	7/19/63, 1030-1330. Recombiner off, nitrogen purge on.	25 ml (1035-1120)	10 ± 1 ml	2.5×10^{-4} μc/ml.
6	7/19/63, 1520-1820. Same conditions as "5."	None	9.4 ± 1 ml	Combined with sample 7.
7	7/19/63, 1930-2230. Same conditions as "5."	None	3 ± 1 ml	Combined with sample 6, 2×10^{-4} μc/ml
8	2330, 7/19/63 to 0850, 7/20/63. Same conditions as "5."	None	3.5 ± 1 ml	No analysis.

Between trapping runs, the sodium system was isolated from the evacuation system and the nitrogen gas addition was continued.

A ninth run of approximately 10 hours duration was made on July 20 with both recombiner and nitrogen purge off, to remove residual moisture from the system and to reduce the system pressure. The amount of water trapped was not measurable.

Four samples of recirculating boiler water, taken from different points in the Power Plant water system on July 18, showed no detectable tritium activity (less than 4×10^{-6} μc/ml).

The tritium activity values given above were completely unanticipated because the environmental tritium activity at the EBR-II site is very low. Samples of EBR-II well water, for example, have never shown detectable tritium activity by the analytical method used, which is capable

of measuring a minimum of 4×10^{-5} μc of tritium activity in a water sample sample volume not exceeding 10 ml Because of these unexpected results, the emphasis shifted to tests which might disclose the source of the tritium activity.

Samples collected on July 19 showed no measurable tritium activity in moisture condensed in cold traps from the atmosphere in the laboratories where the trapping run samples had been handled. A sample of atmospheric moisture collected in the Sodium Boiler Building on July 20 showed a low level of tritium activity: 2.2×10^{-5} μc/ml of atmospheric water.

Samples of water from the same source as that added to the sodium system were analyzed for tritium activity; no measurable activity was present.

On July 22 and 23, a 24-hour trapping run was made on the sodium system to determine trappable system activity without purposeful water addition. The recombiner and nitrogen purge gas were on. No water was evident in the cold trap, but the trap was rinsed twice with tritium-free water, and the rinsings were analyzed; the first and second rinse samples showed, respectively, 3.2×10^{-4} μc/6 ml and 1.1×10^{-4} μc/7 ml.

To isolate the evacuation system itself as the source of tritium activity, an 18-hour trapping run was made on July 24 and July 25 with the evacuation system isolated from the sodium system After nitrogen purge and pump-down of the system, 10 ml of water were added upstream of the recombiner and collected in the cold trap. Accurate measurement of the collected water volume was impossible because the sample contained a large amount of copper oxide sludge which had been carried from the recombiner. The activity of the sample was less than the detection limit, 4×10^{-5} μc.

To determine whether water additions to the sodium system might be washing out the tritium activity, an 18-hour trapping run was made on July 25 and 26 by addition of 25 ml of water and with recombiner and nitrogen purge on. Approximately 23 ml of water was collected in the trap, the measured activity was 2.4×10^{-3} μc per 10 ml, or 2.4×10^{-4} μc/ml The agreement in activity level between this sample and the composite samples from trapping runs 1 through 3 makes attractive a hypothesis that an extensive source of tritium activity exists in the sodium system and that it releases activity at an essentially constant rate

Preliminary to determining whether the large volume of sodium in the secondary storage tank might be the source of the tritium activity, the tank was pressurized with nitrogen to approximately 9 psig on July 25 The freeboard space in the storage tank had been under vacuum since June 19

On July 29, the nitrogen was allowed to flow through a copper oxide recombiner and cold trap for collection (as tritium oxide) of any tritium present in the storage tank freeboard space. As this report is being written, no results are available.

Inasmuch as helium was used for leak testing of the secondary sodium system following construction, it was suspected as a possible source of tritium. To determine whether detectable tritium activity is present, bottled helium was passed through a copper oxide recombiner and cold trap. The trap was rinsed with water and the rinsings were analyzed. No detectable tritium activity was present

The atmospheric moisture samples mentioned earlier were collected in cold traps only; therefore, only tritium oxide would have been collected. To determine whether or not significant amounts of activity as tritium are present in the atmosphere at the EBR-II site, a moisture sample was collected by passage of outside air through a copper oxide recombiner and cold trap. The analytical result, 2×10^{-5} μc/ml of collected water, agreed with that previously obtained for the air in the Sodium Boiler Building.

In view of the unexpected, and relatively high, "background" tritium activity in the secondary sodium system, the efficacy of a tritium leak test, as previously planned, is questionable. The objective of the test was to provide an unequivocal answer as to whether or not a water leak of detectable magnitude exists in the steam generator, based upon the presence or absence of detectable tritium activity in water samples from the system. In view of the relatively high, and ostensibly constant, level of tritium activity in the system, the previously proposed test using tritium tracer could not give a definite answer concerning the existence of a small leak, based alone upon the presence of tritium activity in the sodium system. The best that could be done with the test would be to determine that the magnitude of a small leak is less than some value which depends upon the sensitivity and accuracy of measurement of an incremental tritium activity.

It has been estimated that, with "background" tritium activity of the level observed in the sodium system and with an activity level of about 0.05 μc/ml in the boiler water (3 7 c in the recirculating water volume), the minimum leak rate which can be determined with confidence is about 1 ml per 24 hr.

By comparison, data from the last argon pressurization test, described earlier in this report, indicate an apparent system leak rate between 0 25 ml per 24 hours and 2 5 ml per 24 hours. The former value is based

upon the assumption that only the water vapor in the sodium system came from leakage and that the hydrogen came from an independent source. The latter value is based upon the assumption that both water vapor and hydrogen came from a leak, the hydrogen being formed by reduction of water in the system through corrosion or some other chemical process.

Work is continuing in an attempt to determine the source of the tritium activity in the sodium system. The feasibility of performing a tritium leak test with a high tritium "background" in the system is being investigated.

3. Power Plant

Throughout the month, water circulated through the sodium boiler from the steam system was maintained at 330°F and 1000 psig in the steam drum except during the last week when the water temperature was increased to 345°F to approach the tritium leak test specifications more closely. A closed system mode of recirculation was used throughout the month with heating done by heaters 3 and 4 and all auxiliary steam system condensate returned to the auxiliary boiler. This mode of operation is essential for the tritium leak test.

Sulphite concentration in recirculating water for the first half of the month was between 30 and 95 ppm and pH between 9.7 and 10.4. On July 20, the sulphite concentration was increased to 135 ppm and the pH to 10.4 in preparation for the tritium leak test.

4. Fuel Cycle Facility

The argon purification system turboblower was test-run for 460 hours. Following this run, a bearing inspection showed the equipment to be in good condition.

The periscope at argon cell Window No. 6 was installed and leak-tested. Satisfactory results were obtained from both the optical system and the gas seal.

A pair of sealed master-slave manipulators were installed at argon cell Window No. 2. The through-tube and transfer box for an additional arm at Window No. 15 was installed.

Modifications to the method of removing and replacing the cable of the argon cell electromechanical manipulator were devised and successfully accomplished.

Installation of the air cell dismantler was completed. Trial runs with the machine indicated the need for some field modifications; these are under way. Work has continued on the installation and checkout of the pin processing machine and the welders.

The square telescoping tubes of the electromechanical manipulator, which had exhibited some galling, have been modified. The modification consisted of the replacement of alternate steel sections with brass.

The fabrication of the 20-ton interbuilding fuel transfer coffin which was designed by ANL personnel and built at Argonne was completed. The fuel transfer coffin will be used for transferring spent or reconstituted EBR-II fuel subassemblies between the Reactor Building and the Air Cell of the Fuel Cycle Facility. The motor-blower assembly for recirculating the cooling gas (air or argon) through an EBR-II fuel subassembly operates satisfactorily from the storage batteries contained on the coffin (see Progress Report, January 1963, ANL-6683, page 13). Heat removal performance tests have been conducted using a mock-up heated subassembly. This subassembly is similar in construction to a standard core subassembly except that the core section pins were replaced by heaters. A heat load of 1050 watts is the estimated heat output of a subassembly for 2 percent burnup and 15 days cooling. A maximum center pin temperature of 600°F is a performance requirement of the coffin cooling system. The results of the heat removal performance tests have shown that, for air flow rates between 1 and 30 scfm and for heat loads between 341 and 1500 watts, the center pin temperature could be maintained at 600°F or lower. The fuel transfer coffin has been shipped to the EBR-II site in Idaho.

All shielding windows in the Air Cell and Argon Cell have now been provided with steel shielding window shutters. Slip clutches of ANL design (see Progress Report, February 1963, ANL-6698, page 19) have been installed on all shutter drive units. Use of the slip clutches has eliminated the chatter in the shutter drives which occurred at the end of the shutter travel because of the high stalling torque of the drive motors.

Calculations of temperature profiles through the glass slabs in the 60-in. thick shielding windows have been made. Temperature gradients occur within a glass window as a result of the absorption of the gamma energy to which the window is exposed under plant operating conditions. The effect of steel shielding window shutters on the temperature profile was also calculated. The following conditions during cell operations were assumed for the calculations: a radiation intensity of 5×10^5 rad/hr, a cell ambient temperature of 100°F, and an outer annulus temperature of 70°F. With the steel shielding window shutter open, the calculated temperature profile at equilibrium shows that the temperature in the shielding window rises to a maximum (175°F) at about 5 in. from the cell side (A slab).

With the steel shielding window shutter closed, the calculated temperature profile at equilibrium shows that the temperature at the face (cell side) of the shielding window is 140°F and then slowly decreases through the shielding window to the ambient outer annulus temperature (70°F)

In an effort to obtain a measure of the reliability of tungsten as a containment material for molten uranium, two small crucibles were fabricated from tungsten and tested while containing uranium One crucible, about 1 in. in diameter and 1 in. high, was made from swaged tungsten rod. In a 50-hour holding test at 1200°C, this crucible was attacked to a maximum depth of 4 mils. The other tungsten crucible, which had been fabricated by slip casting and then sintering, disintegrated rapidly (failed in 30 minutes) when used to hold molten uranium at 1200°C.

5. Process Development

a. Melt-refining Process Technology In the EBR-II melt-refining process for separating recycled fuel from volatile fission products, fission product iodine collects on the cylindrical Fiberfrax fume trap over the melt refining crucible, apparently in the form of cesium iodide Heat from the decay of sorbed fission products and of fission products remaining in the skull might raise the temperature of the Fiberfrax trap sufficiently so that some of the iodine might be released to the atmosphere of the Argon Cell upon opening of the melt refining furnace. In the present study, one-inch diameter Fiberfrax plugs were heated to various temperatures to simulate two typical conditions of fission product decay heating, and the amounts of iodine desorbed were measured The plugs employed in these experiments had been used in the melt refining of mildly irradiated uranium-fissium charges containing iodine-131 and cesium-134 The desorbed iodine was swept out of the system in a stream of argon gas which was then passed through a filter assembly consisting of a charcoal bed with a high-efficiency filter at each end Data on the release of iodine have now been obtained at 170°C (to simulate the situation where the fume trap is lifted from the melt refining crucible) and at a gradient of 315 to 680°C between the ends of the Fiberfrax (to simulate the situation where the fume trap is resting on a crucible containing active skull material) Iodine activities collected in the filter assemblies were as follows

Iodine Collection Time (hr)	Fiberfrax Temp (C)	O_2 Content of Argon (ppm)	Total I^{131} in Fiberfrax (μc) at Start of Iodine Collection	I^{131} (μc) in Filter Assy at End of Iodine Collection
34.2	315-680	2	867 5	47 7
30.2	170	2	307.8	0.009
30.9	170	175		0.020

These results indicate that the rate of release of iodine activity to the Argon Cell of the Fuel Cycle Facility will not constitute a serious problem.

b. Skull Reclamation Process. The skull reclamation process will be used to recover and purify the fissionable material in the crucible residue (skull) remaining after a melt refining operation. Small-scale (100 grams of uranium) process demonstration runs are being made to optimize process conditions and resolve process problems. In one recently completed run, the 139-gram charge consisted of 90 percent unoxidized skull and 10 percent skull oxide, to which was added a pin of irradiated uranium as tracer; in another completed run, the 101-gram charge consisted of fully oxidized skull material to which was added ruthenium-106 as tracer. Material balances showed uranium losses in the two demonstration runs to be only 1.6 and 2.2 percent, respectively, based on the assumption that the uranium present in heels and in analytical samples is recoverable. These losses are smaller than the allowable value of about 5 percent. The fission product removals were satisfactory, except for a low removal of zirconium (56 percent) in the first run.

Operation of the large-scale (2.5 kg skull oxide) integrated skull reclamation processing equipment was continued. Work with this equipment will provide an evaluation of equipment and process performance at nearly full plant scale. The equipment has been modified to permit all steps of the skull reclamation process except the final retorting step to be performed in a tungsten crucible in either of two furnaces. Following this, an additional run was made in which pressure-siphoning of liquid phases from the tungsten crucible was accomplished without major difficulties. However, there is need for achieving more nearly complete removal of waste metal and waste salt phases, especially in the step in which the supernatant metal phase is removed after precipitation of the uranium-zinc intermetallic compound.

Distillation equipment is being tested for the removal of residual magnesium-zinc from uranium in the last step of the skull reclamation process (see Progress Report, March 1963, ANL-6705, page 28). A new distillation unit, which can be used with the melt refining furnace base, has been designed. This unit, which consists of a distillation crucible, a vented crucible cap, and a disposable collector-condenser, was used to make six runs. A butt-type seal which was used between the disposable collector-condenser and the vented crucible cap was tested to determine the effectiveness of the seal in preventing distilled molten metal from entering the annulus between the collector and the crucible cap. Three runs were carried out in which 1000 g of 14 w/o magnesium-86 w/o zinc was charged to the crucible in each run. Three additional runs were made in which 3000 g of the same alloy was used in each run. The distillations were carried out under reduced pressure (1 mm Hg) at final crucible

temperatures between 1200 and 1250°C. The butt-type seal proved satisfactory in all runs. There was no measurable leakage of distilled metal. At the end of each run the condenser collector could be readily removed from the crucible; no sticking between these two components was encountered.

A study (see Progress Report for May 1963, ANL-6739, page 25) to determine whether the noble metal extraction step of the skull reclamation process can be adapted to the removal of uranium from various cladding materials is being continued. In recently completed runs on a 20-g scale, 0.144-in. diameter by 1 to 1.5-in. long clad uranium-5 percent fissium pins were contacted with zinc-salt* mixtures for 4 hours at 750°C. The total uranium (dissolved uranium and undissolved uranium) retained in the waste metal phase at the end of the runs for the various pin claddings were (percent of the uranium charged): 304 stainless steel, 10.0; tungsten-coated Hastelloy X, 15.7; tungsten-coated 304 stainless steel, 24.4; and niobium-1% zirconium, 34.8. To aid in the interpretation of results, it is desirable to know the amount of uranium that was in solution in the zinc phase and the amount of zinc chloride that was left in the molten salt phase when each run was terminated. This information will be available when the analyses of appropriate samples of the molten metal and salt phases are completed.

c. Blanket Processing Studies. Work is proceeding on an alternative blanket process for the isolation of plutonium from uranium blanket material. In this process uranium and plutonium are first oxidized into a flux phase with zinc chloride and subsequently reduced from the flux phase with magnesium. The plutonium dissolves in excess magnesium, which floats on the flux, while uranium precipitates to the bottom of the crucible. Work is being carried out in an effort to improve the separation of the phases. The effects of changes in process conditions and flux composition are being studied. The addition of alloying agents to increase the coalescence of uranium is also being investigated.

d. Liquid Sodium Coolant Chemistry. An activation method that depends on the $O^{16}(n,p)N^{16}$ reaction is being explored for the determination of 10 to 100 ppm oxygen in sodium metal (see Progress Report for March 1963, ANL-6705, page 47). The success of this method depends to a large extent on finding suitable low-oxygen containers for the sodium during the irradiation and analysis of the induced activity. Preliminary studies are underway to evaluate polyethylene and other potential container materials.

---

*The salt extractant was 47.5 m/o calcium chloride-47.5 m/o magnesium chloride-5.0 m/o magnesium fluoride plus an amount of zinc chloride either 20 or 100 percent in excess of the stoichiometric requirement to oxidize the uranium.

6. Training

A reactor technology course convened on July 15 for new technicians for various Idaho Division projects. This course is scheduled for half-day sessions daily and will cover a minimum of 130 hours of work.

On July 15, shift supervisors were relieved of shift duty for three and one-half weeks of training. The purpose of this training was to up-date the shift supervisors with recent plant modifications and qualify them for wet critical operation. This instruction will cover technical and administrative subjects related to wet critical experiments and approach to power.

EBR-II facility and plant orientation class started on July 22 with 16 technicians participating on a half-day basis. Facility orientation was completed on Friday, July 26.

E. FARET

1. Construction Program

Final details are being worked out between ANL and the Bechtel Corporation for architect-engineering services for the FARET facility. A preliminary agreement on the contract between the Laboratory and the Bechtel Corporation was reached in June, 1963.

Title I work was initiated on June 17, 1963, based on the assumption of early approval of the final contract by the Commission.

In joint meetings with Bechtel personnel the interface between the areas of ANL and Bechtel design responsibility was explored in some detail. The function of the facility was reviewed and the over-all operating requirements described. The availability and applicability of computer codes and associated information, particularly for use in the design of the shielding and the reactor coolant system control stability problems, was covered. The experimental program was also briefly discussed. The proposed FARET site at NRTS was visited. The availability of utilities and services from the EBR-II site was investigated; site conditions were discussed, and local labor conditions and costs were reviewed. Discussions were also held on Plant Engineering and AEC standards, codes, practices, and procedures.

An interdivisional review is being made on the conceptual design described in the Feasibility and Cost Study Report (AI-8040). It is not anticipated that information developed during these reviews will affect the Title I schedules. The principal areas being reviewed are:

a. Cell layout and equipment arrangement especially as related to reactor operation and fuel handling considerations.

b. Vault layout, with respect to equipment location and considerations involving primary piping arrangement.

c. Cell and vault space cooling considerations.

d. Design of reactor coolant system.

e. Material selection.

f. Safety analysis, with particular emphasis on the effects on the containment structure of sudden energy releases in the center of the reactor.

A critical path analysis of FARET design and construction has been undertaken by the Laboratory and has progressed to the point where the first results necessary to compute the course and duration of the path are available. The network diagrams currently cover approximately 1700 activities.

2. Fuel Elements for Zoned Test Core

Gas gap conductance for the zoned-core Doppler experiments has been measured for insulated fuel pellet elements using a bench test element (ANL-6672, December, 1962). A number of the measurements were made with air in the gap between pellets of lava material and stainless steel cladding. Typical temperature measurements at a linear heat flux of 20 w/cm showed 860°C at the pellet thermocouple and 450°C at the clad surface, from which a temperature drop of 283°C is calculated across the gas gap.

Subsequently, thermal cycle tests have been conducted on UO_2 specimens to determine their resistance to cracking. The pellets were cycled 10 times between linear heat fluxes of 12 w/cm and 2.2 w/cm by means of a tantalum heater in an argon gas environment. The results of these tests are shown in Table IV.

Table IV. Summary of Initial Insulated UO_2 Pellet Tests

Spec. No.	No. Cycles	Cycle Period, min.	Max. Linear Heat Flux w/cm	Corresponding Reactor Conditions		Min. Linear Heat Flux w/cm	Results
				Heat Flux w/cm	Power Mw*		
2	10	30	12	19.8	4.3	2.2	X-rays show no damage
2	10	25	14.5	23.9	5.2	2.2	Pellet broken (see Figure 3)
3	10	30	12	19.8	4.3	2.2	X-rays show no damage
3	10	25	14.5	23.9	5.2	2.2	Pellet broken
7	10	60	13	21.5	4.7	2.2	X-rays and neutrons show no damage
7	10	60	14.5	23.9	5.2	2.2	Pellet broken
8	10	60	13	21.5	4.7	2.2	X-rays and neutrons show no damage
8	10	60	14.5	23.9	5.2	2.2	Pellet broken

Based on $\frac{\text{max.}}{\text{ave.}} = 1.5$, 1400-1 core

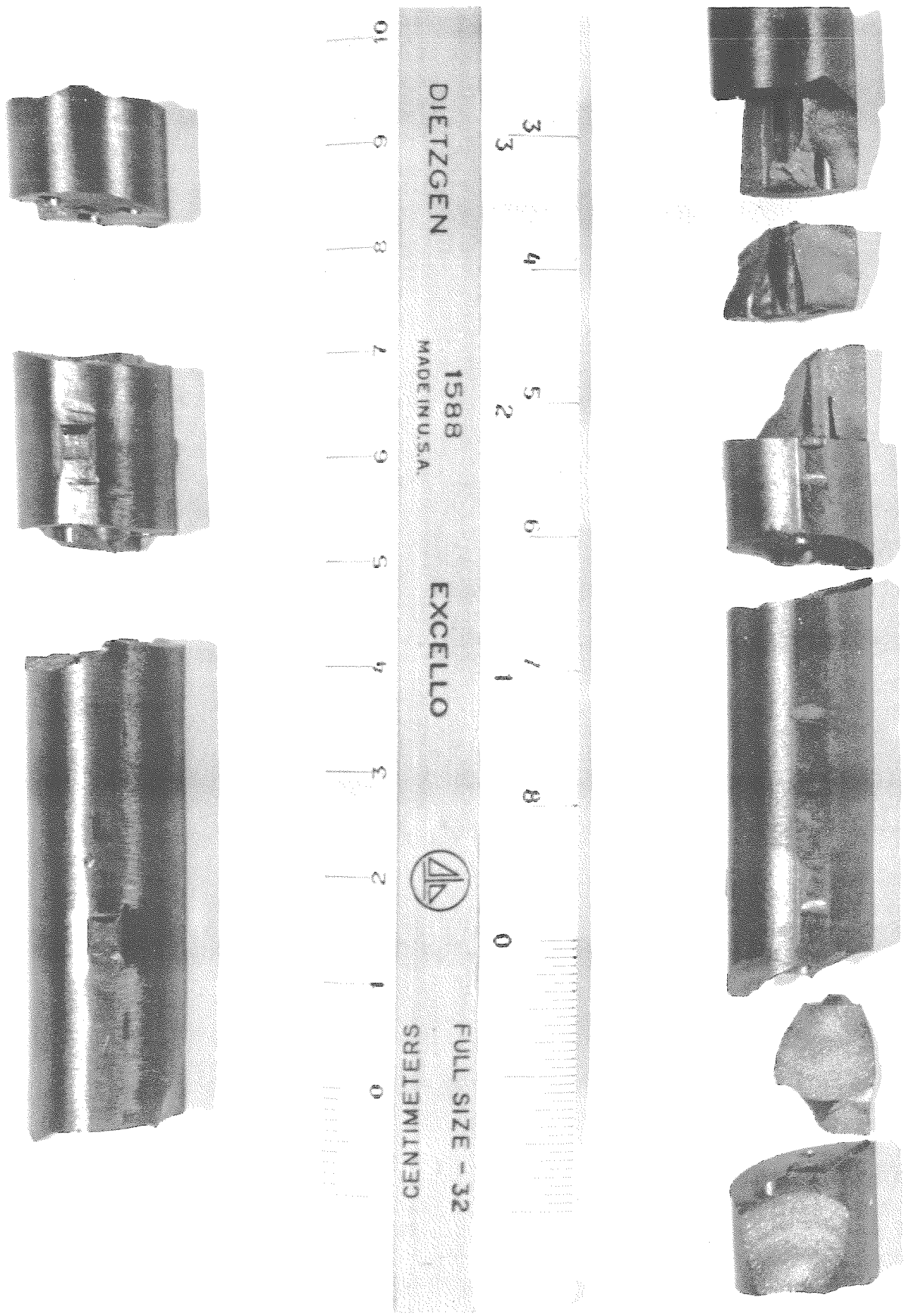

Figure 3. Specimens No. 2 (left) and No. 3 after 20 Thermal Cycles

The thermal conditions during these cycling tests are shown in Table V.

Table V. Conditions in Test Element No. 2 During UO_2 Fuel Pellet Cycling Operation

Linear Heat Flux,[1] w/cm	Pellet I.D Temp,[1] °C	Pellet O.D. Temp,[1] °C	Pellet Thermocouple Temp,[2] °C	Clad Temp,[2] °C
12.0	905	790	820	620
2.2	460	440	-[3]	400
14.5	955	815	850	610

[1] Calculated

[2] Measured

[3] Potentiometer did not indicate temperatures below 550°C

The results of the preliminary tests showed the average test zone linear heat flux may have to be kept below approximately 23.9 w/cm to prevent serious cracking of the pellets. This heat flux corresponds to a FARET power level of about 5 2 Mw.

Succeeding tests will be conducted to establish the maximum heat flux below which the reactor experiment should operate. Simultaneously, efforts are underway to subject the pellets to nuclear heating in the CP-5 reactor.

The integrity of the pellets containing about 10 w/o plutonium will be investigated.

Due to the better thermal conductivity, it is expected that UC will be more resistant to cracking than the UO_2. A backup test using UC will also be undertaken

3. Core Design

Core subassemblies have been designed that will permit variation in fuel element diameter and length for the various core loadings of interest. Figure 4 illustrates the reference subassemblies for a zoned core loading.

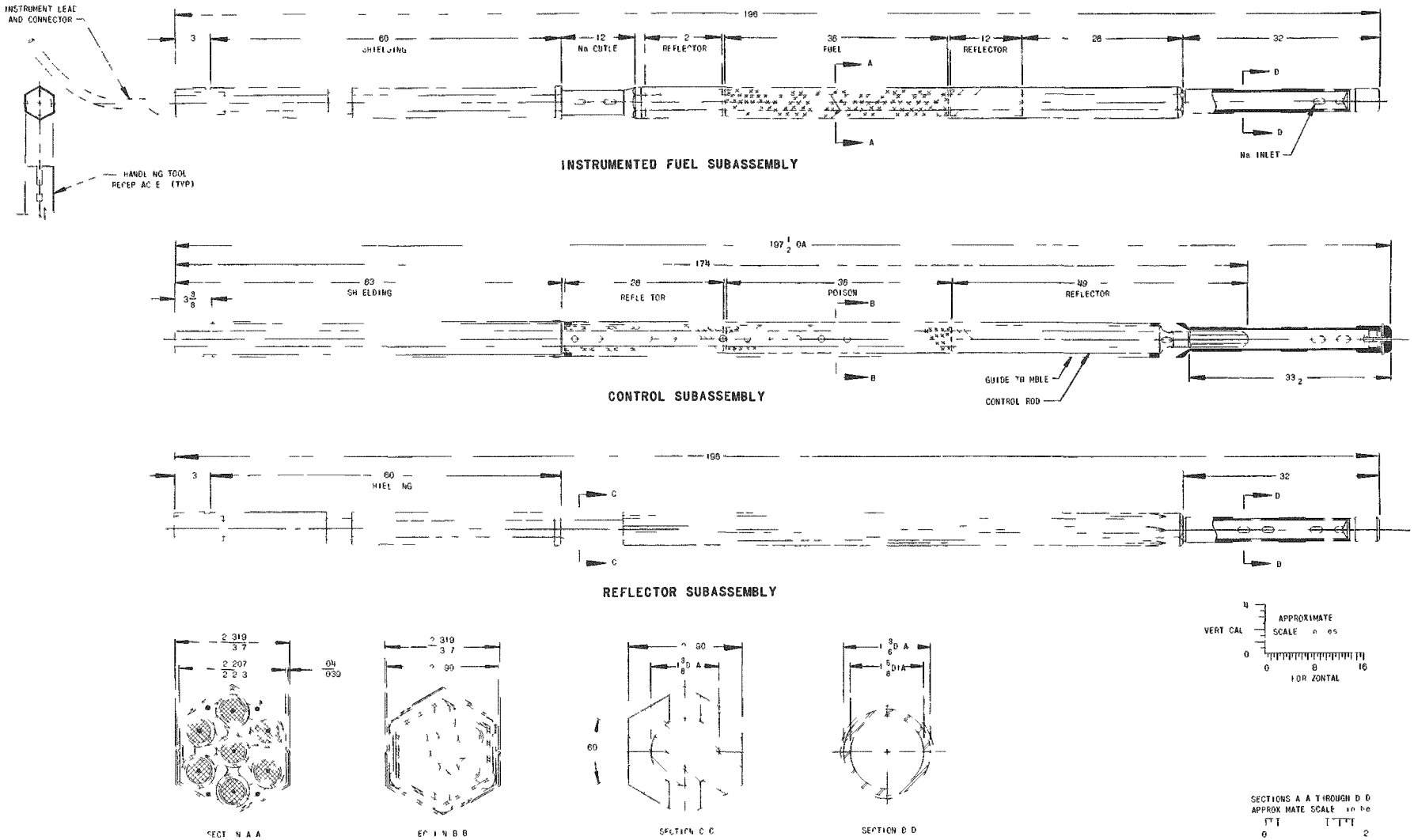

Figure 4. Reference Subassemblies for a Zoned Core Loading in FARET

4. Core Grid Structure

An analysis of the deflection and stresses in the grid structure under thermal and mechanical loads has been made. A thermal gradient, with linear variation through the thickness of the plate and distributed axial symmetrically over the plate plan-form, and a laterally applied pressure were assumed for the analysis. A convergent power series expansion was assumed to express temperature. Classical small deflections theory and the concept of "equivalent solid plate" have been used. A solution has been obtained for a plate with any arbitrarily restrained rotations. Preliminary calculations have been made for a particular loading condition consisting of the following:

a. A total dead weight of 90,000 lbs (595 core elements)

b. Pressure in inlet plenum = 0

c. A transient temperature increase of 300°F from the edge of the plate to the center of the plate.

The maximum deflections for a stainless steel plate (66 in. dia.) at a temperature of about 1,200°F vs plate thickness for various restraint conditions are listed in Table VI.

Table VI. Deflections of Core Support Model

Plate Thickness (in.)	Deflections (in.) for Various Types of Support		
	k* = 0 (Simply Supported)	k = 0.5 (Partially Restrained)	k = 1 (Built-in)
11	0.132	0.088	0.041
6	0.249	0.162	0.141
2	0.684	0.444	0.202

*k - rotational restraint factor $0 \leq k \leq 1$.

Computations for more realistic loading conditions will be made in the near future.

The study of creep bending of perforated circular plates at elevated temperatures has been initiated. It appears that there is a lack of comparable information available to permit an interpretation of creep phenomena in a satisfactory manner for this application. Work on this is continuing.

5. In-pile Experiment

Instrument requirements for the CP-5 in-pile experiment of fuel pellets for the zoned loading have been formulated. One of the major problem areas is the clad temperature vacuum control system and the fuel-gas-gap vacuum control system. An analysis of the out-gassing problem and the pressure control system will be made. A mockup control system will be built and tested.

Specifications for the clad surface and heat flow transducer thermocouples have been written. The specifications for the fuel pin thermocouples will be written and a requisition placed for all thermocouples.

6. In-vessel Connectors

A preliminary prototype connector design is shown in Figure 5. Each connector can accommodate sixteen sensors, assuming each sensor requires a pair of wires. The design permits remote assembly of the plug and receptacle.

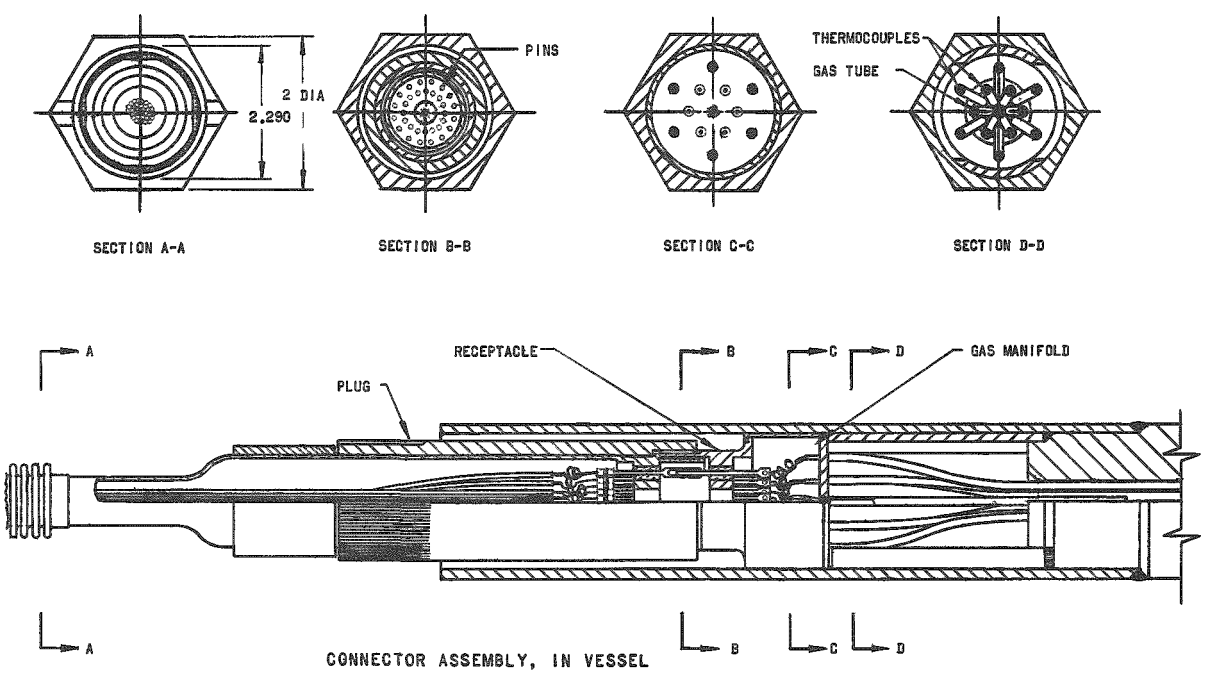

Figure 5. Preliminary Prototype Connector Design for Use in FARET

The rig for testing connectors have been fabricated and assembled. Sample connectors are now available. The high temperature cable has also arrived but has not been completely checked out. Testing should commence soon.

Full-scale mockup connectors and in-vessel leads are being made It is planned to include nine connectors and leads in the FARET mockup vessel

7. In-core Instrumentation

It has become apparent that base-metal extension lead wire must be developed for use with the tungsten-rhenium alloy thermocouples when the junction of the lead and thermocouple wire is made in the 250 to 650°C temperature range. Extension lead wire is available for use from room temperature up to 250°C. The development of high temperature lead wire is being investigated with a number of vendors.

III. GENERAL REACTOR TECHNOLOGY

A Applied Nuclear Physics

1. Fast Neutron Scattering

Time-of-flight measurements of elastic and inelastic scattering cross sections have proceeded on a routine basis. The increasing application of on-line digital computer systems has not only speeded the work but grossly improved the experimental precision. The time resolution has been improved by a factor of two and the sensitivity extended to a cutoff of less than 100 kev. Measurements brought to a formal conclusion during this period include the determinations of the differential elastic and inelastic scattering cross sections of Cu and Zn (E_n = 300 - 1500 kev). The elastic results shown in Figures 6 and 7 are representative of the work

The Progress Report for June (ANL-6749, p. 26) discussed some trends in elastic and inelastic cross sections as determined from these measurements. These systematics are becoming clearer as more information is obtained. This is illustrated in Figure 8. Here the differential elastic cross section is shown as a function of incident neutron energy and mass number. As in previously recorded data, the effect of closed nuclear shells is clearly seen. The systematic dependence of cross section on incident energy is also evident. Using information such as that shown in Figure 8 it is possible to derive the systematic behavior of cross sections and, thus, predict values for nuclei not amenable to measurement. Such an evaluation of the systematics is now in progress. The ultimate objective is a cross sectional library which can be directly utilized as input information in the calculation of the performance of fast reactor systems.

2. Neutron Capture Cross Sections

The neutron capture cross section for Ta^{181} was measured utilizing activation techniques. Absolute cross sections for neutron capture from 175 kev to 1500 kev were determined from comparison measurements with thermal neutrons for both the 115 d and 16.4 m activities. The neutron capture cross section associated with the 16.4 m activity remained between 1 mb and 2 mb throughout the entire energy range covered. Thus, the 115 d activity accounted for most of the neutron capture cross section. The total neutron capture cross section, obtained by combining the activation cross sections for the 115 d and 16.4 m activities, is given in Figure 9 together with the measurements Diven, et al.[1] and Gibbons, et al [2] It is evident from the figure that our results are in much better agreement with those

[1] B. C. Diven, J. Terrell, and A. Hemmendinger, Phys. Rev. 120, 556 (1960).

[2] H. Gibbons, R. L. Macklin, P. D. Miller, and J. H. Neiler, Phys. Rev. 122, 182 (1961).

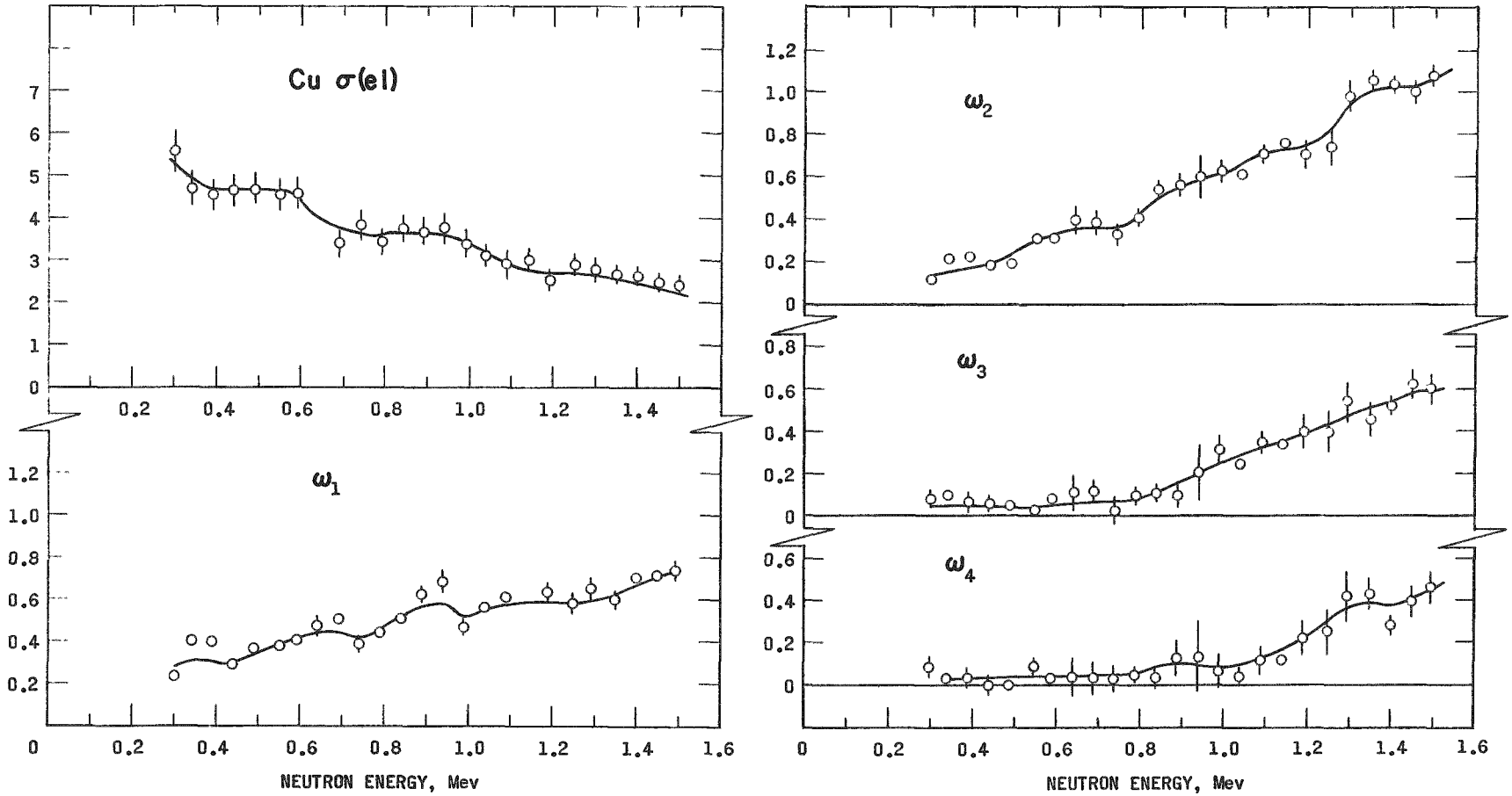

Figure 6. Elastic Differential Cross Section of Copper Expressed in Form

$$\frac{d\sigma}{d\Omega} = \frac{\sigma}{4\pi}\left[1 + \sum_{i=1}^{4} \omega_i P_i\right]$$

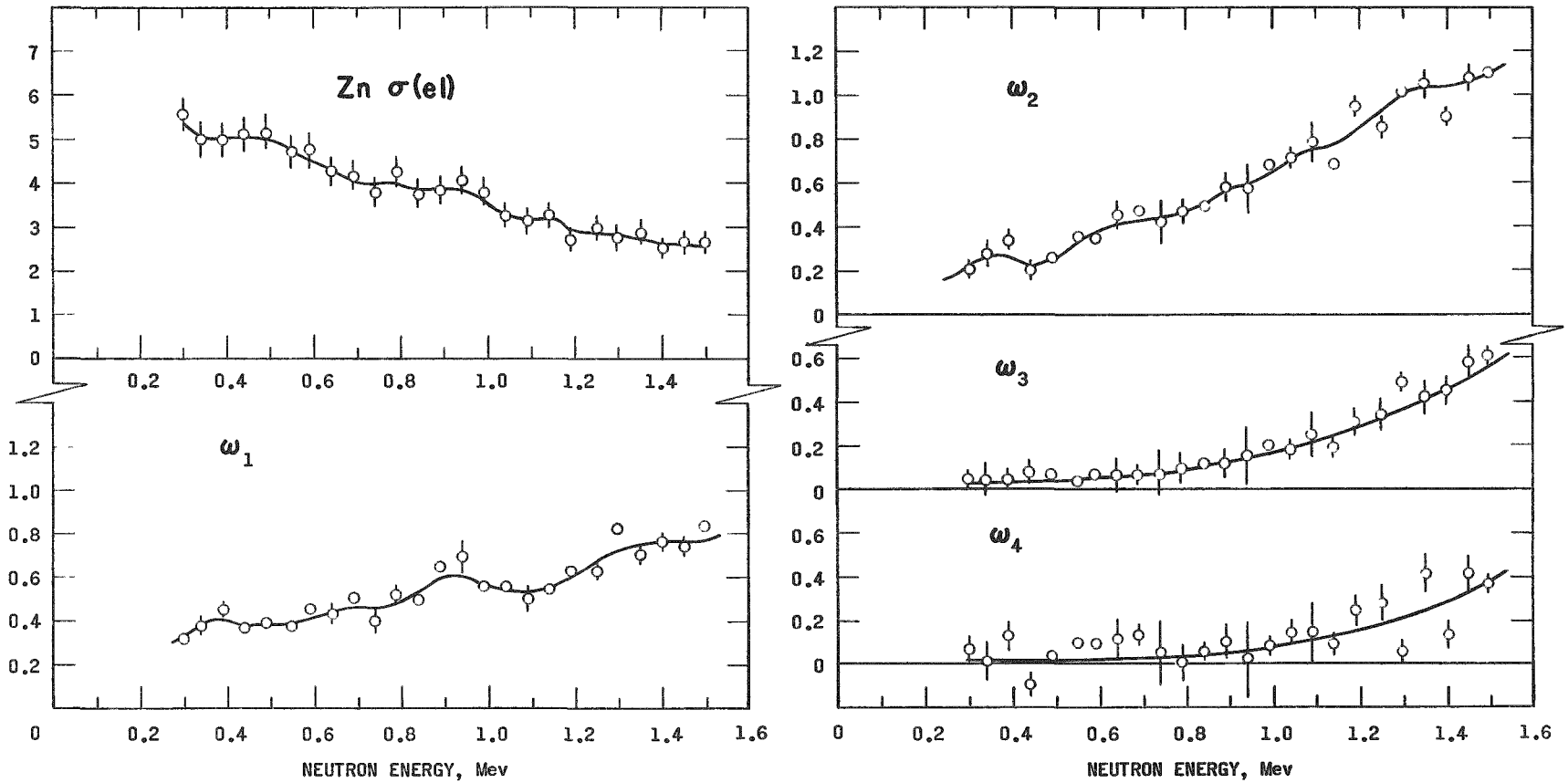

Figure 7. Elastic Differential Cross Section of Zinc Expressed in Form

$$\frac{d\sigma}{d\Omega} = \frac{\sigma}{4\pi}\left[1 + \sum_{i=1}^{4} \omega_i P_i\right]$$

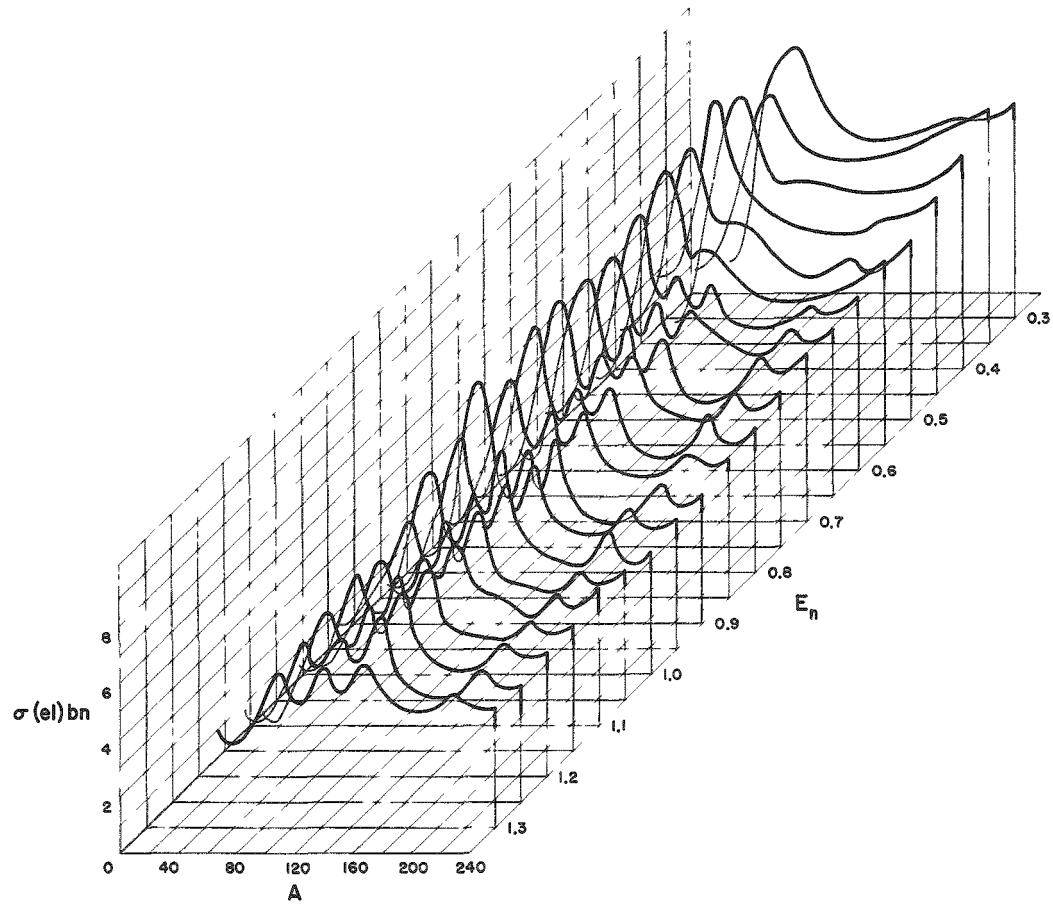

Figure 8. The Total Elastic Cross Section as a Function of Incident Neutron Energy and Target Mass Number.

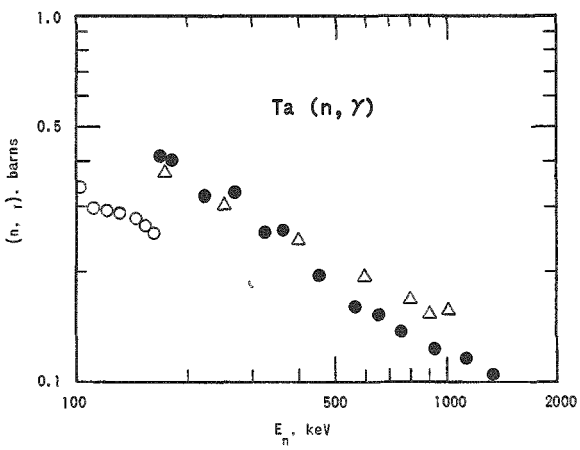

Figure 9. Neutron Capture Cross Section for Ta^{181}. The data are from this experiment (●); Diven, et al., △; and Gibbons, et al., (○).

of Diven, et al., than with those of Gibbons, et al. Our previously reported results for bromine, rhodium, indium, and iodine were also in good agreement with those of Diven, et al., and in poor agreement with those of Gibbons, et al.

3. On-Line Computer for Data Analysis

A versatile display unit for the 160-A computer has been completed and is now in operation. Display is on a 5-in. oscilloscope. Two-dimensional displays of up to 512 channels are available. Overlapping displays of any section of the computer memory may be had by appropriate programming. The three-dimensional display allows selection of

a cross sectional slice or a specified contour. Location of the slice or the contour is set by switches on the display unit. An isometric view is also available.

4. High Conversion Critical Experiments

The critical dimensions, reflector savings, and the bucklings derived from measurements made in the 1.27-cm triangular and 1.24 cm square lattice HiC assemblies are shown in Table VII. Data, such as the fast fission factor, thermal utilization, the resonance escape probability, and the initial conversion ratio (ICR) are being evaluated. A systematic investigation is being made of pertinent corrections to be applied to the measurements. A cylindrical zone of approximately 400 stainless-steel-clad, HiC fuel pins was loaded into the center of the 1.27-cm triangular, aluminum-clad in order to measure the microparameters in a stainless steel environment. Thus far, data have been obtained for ϵ and f and one irradiation made for both ρ^{28} and ICR.

Table VII. Critical Parameters and Buckling Measurements in Lattices of Aluminum-Clad HiC Fuel

Lattice	1.27 cm △	1.24 cm □
H/U^{238} atom ratio	2.30	2.93
Critical No. of fuel pins	1417 ± 3	950 ± 1
Clean Critical Radius, cm	25.10 ± 0.03	21.56 ± 0.02
Radial reflector savings, cm	8.77 ± 0.07 (11)*	8.13 ± 0.16 (8)*
Extrapolated radius, cm	33.87 ± 0.08	29.69 ± 0.16
Radial buckling, $cm^{-2} \times 10^4$	50.42 ± 0.24	65.61 ± 0.71
Axial reflector savings, cm	19.11 ± 0.18 (4)*	16.52 ± 0.31 (4)*
Extrapolated height, cm	141.03 ± 0.18	138.44 ± 0.31
Axial buckling, $cm^{-2} \times 10^4$	4.96 ± 0.01	5.15 ± 0.02
Buckling, $cm^{-2} \times 10^4$	55.38 ± 0.24	70.76 ± 0.71

*Indicates number of measurements

The change in reactivity with buckling, $\partial\rho/\partial B^2$, for the HiC cores to date was estimated from the experimental determination of peripheral fuel pin worths and the change in the number of fuel pins with buckling as computed for the clean, critical core, holding the axial buckling constant. The migration area was inferred from the modified one-group expression

$$M^2 = \frac{-\partial\rho/\partial B^2}{1 + B^2 \partial\rho/\partial B^2}$$

The results of this calculation for the HiC cores are given in Table VIII. Anisotropy in the migration area was not considered. The degree of precision in Table VIII is in part a result of $7\frac{1}{2}\%$ error assumed for the peripheral fuel pin worth.

Table VIII. Migration Areas of HiC Cores

Lattice	$\partial\rho/\partial n$ Peripheral Fuel Pin Worth Reactivity per Pin x 10^6	$\partial\rho/\partial B^2$ Reactivity per cm^{-2}	M^2 Migration Area, cm^2
1.24 cm square SS clad	70 ± 5.2	-37.1 ± 2.8	45.0 ± 4.1
1.24 cm square Al clad	168 ± 12.6	-33.5 ± 3.5	43.9 ± 4.3
1.27 cm triangular Al clad	112 ± 8.4	-42.5 ± 3.2	55.5 ± 5.6

5. Theoretical Physics

a. Numerical Methods Analysis. One of the most economical methods for storing mathematical functions in the computer is by the coefficients of their expansions in Chebyshev polynomials. In contrast to storing the coefficients of the equivalent ordinary polynomial, one set of coefficients serves for any desired accuracy up to the maximum, and the accuracy obtained is easily determined from the magnitude of the coefficient of the first term neglected. Although the coefficients may be obtained by rearranging the terms of the power series, difficulties are encountered when the power series does not converge rapidly, and other methods have normally been used to obtain them.

Promising results have been obtained for slowly converging series by use of the Euler summation transformation. Let the function for which the Chebyshev series is desired be given by:

$$f(x) = \sum_{j=0}^{\infty} a_j x^j \qquad (1)$$

and let $\nu_{j,k}$ be the coefficient in the expansion of x^j in Chebyshev polynomials:

$$x^j = \sum_{k=0}^{j} \nu_{j,k}\, T_k(x) \qquad (2)$$

Then,

$$f(x) = \sum_{j=0}^{\infty} a_j \sum_{k=0}^{j} \nu_{j,k} T_k(x) = \sum_{k=0}^{\infty} \left\{ \sum_{j=k}^{\infty} a_j \nu_{j,k} \right\} T_k(x) \qquad (3)$$

The Euler transformation is then applied to the summation over j to obtain the desired coefficient. The same procedure may clearly be applied to obtain coefficients for the shifted polynomials, $T_k^*(x)$. Moreover, the Euler transformation may be replaced by any of the other standard devices for improving the convergence.

To test this approach, it was applied to the series

$$\ln(1+x) = -\sum_{j=1}^{\infty} \frac{(-x)^j}{j} = \sum_{k=0}^{\infty} b_k^* T_k^*(x) \qquad (4)$$

Using only the first 10 terms in the power series (which would only be good to 0.05), a Chebyshev expansion good to less than 10^{-6} was obtained.

b. Doppler Effect Studies. The total Doppler effect of an oxide-fueled reactor with 52 v/o sodium, 32 v/o fuel, and 16 v/o steel has been computed for fuel containing U^{238} and Pu^{239} in various ratios. The positive Pu^{239} contribution as a percentage of the negative U^{238} contribution has also been obtained. The results are given in Table IX. It is seen that a negative effect is still obtained at a U^{238}/Pu^{239} ratio of 2, although the total Doppler effect has become quite small by this time. The fact that the Pu^{239} effect as a percentage of the U^{238} effect does not increase more rapidly with decreasing U^{238}/Pu^{239} ratio is due to the fact that the U^{238} Doppler effect becomes more appreciable with increase in neutron energy than does the Pu^{239} effect because the resonances are stronger. As the low energy spectrum hardens because of increasing fissile material concentration, the U^{238} effect thus is still dominant. It seems unlikely that a positive Doppler effect will ever be a significant problem in an unmoderated power reactor.

Table IX. Doppler Effect of Oxide Fueled Reactors as a Function of U^{238}/Pu^{239} Ratio

	Total ($-\delta k$)			Positive Pu^{239} Effect as Percentage of Negative U^{238} Effect		
U^{238}/Pu^{239}	300-750°K	750-1500°K	1500-2500°K	300-750°K	750-1500°K	1500-2500°K
9	1.17	0.87	0.59	14	13	13
7	0.72	0.53	0.38	19	17	15
5	0.38	0.28	0.20	24	23	19
3	0.092	0.068	0.045	42	38	38
2	0.032	0.025	0.016	44	41	41

The above calculation used the following parameters for Pu^{239}: $\langle \Gamma_n^0 \rangle / D = 1 \times 10^{-4}$, $\langle \Gamma_f \rangle = 0.099$ ev, 2 channels per fission, level spacing 11.6 ev for J = 0, 3.86 ev for J = 1. It was pointed out in the June Progress Report (ANL-6749) that reasonable variations of the first three parameters did not make much difference in the results. It was recently discovered[3] that a significant interaction effect of U^{238} on some of the Pu^{239} resonances exists which may change the Pu^{239} Doppler effect from positive to negative. This is still under study and has not been taken into account in the present work.

c. ZPR-VII Data Analysis. The cylindrical cell collision probability program (see ANL-6683, Progress Report for January 1963) has been extended to three regions. Calculations of thermal flux disadvantage factors for the BORAX-V square and triangular lattices using this code give results in rather close agreement with those derived using either the 30-group THERMS code or the one-group THERMS code. In both the THERMS and 1692/RE one-group problems the cross sections used were derived from the multigroup THERMS output. To obviate the mirror image reflection boundary condition in THERMS, a region three mean free paths thick consisting of a heavy scatterer was placed outside the actual unit cell.[4]

The 1692/RE code has also been used to calculate disadvantage factors for some lattices previously studied by Thie (Ref. 5, lattices 1, 4, 6). Values of D-1, where D is the disadvantage factor, are about 2 to 4% lower than those obtained from S_{16} calculations using the Winfrith DSN code with "white" boundary conditions. The nature of the flat flux approximation in 1692/RE is such that the disadvantage factors should be slightly low.

THERMS multigroup problems are being done for the HiC square and triangular lattices with both aluminum and stainless steel clad. For these problems, and the BORAX-V problems mentioned above, the free gas, Brown-St. John, and Nelkin scattering kernels are all being used for hydrogen. The Nelkin kernel yields the hardest spectrum, while the Brown-St. John spectrum is a little softer than that produced by the free gas kernel. However, the difference in thermal parameters such as η and f produced by the three

---

[3] J. Codd and P. Collins, "Pu^{239} and U^{238} Resonance Interaction Effects in a Dilute Fast Reactor," E.A.E.S. Symposium on Advances in Reactor Theory, Karlsruhe, April, 1963.

[4] H. Honeck, "Some Methods for Improving the Cylindrical Reflecting Boundary Condition in Cell Calculations of the Thermal Neutron Flux," TANS Vol 5, No. 2, p. 350 (November, 1962).

[5] J. A. Thie, "Failure of Neutron Transport Approximations in Small Cells in Cylindrical Geometry," Nuc. Sci. Eng. 9, No. 2, p. 286, (February, 1961).

kernels are not very large, and are much smaller than the differences between the free gas and Radkowsky results in SOFOCATE. This is because the Radkowsky kernel produces a much harder spectrum than any of the others.

d. Multigroup Constants Code. A subroutine to compute inelastic scattering matrices for a given lethargy width has been written. This subprogram requires that the cross sections for excitation of the inelastic levels be represented as linear segments on a log-log plot. Above a specified energy the code uses the statistical model to compute inelastic transfers.

A subroutine to generate a fission spectrum source for an arbitrary number of groups of constant lethargy width over a given energy range has been written. The program assumes that the group fission spectrum can be represented by a function of the type

$$F_j = A\int_{\text{group } j} e^{-BE} \sinh \sqrt{CE}\ dE \quad .$$

An analytic representation for the integral is used in the program. The code uses a rational approximation due to Hastings for the terms involving the error function.

The elastic scattering routine for the master code has been taken from the ELMOE code. Modifications have been made to remove the restriction in ELMOE that all scatterers must scatter an integral number of groups. This will permit the treatment of heavy scatterers correctly. ELMOE at present redefines the mass of the scatterer to make all materials scatter an integral number of groups.

A subroutine for the calculation of a weighting spectrum has been written, using the ordinary P-1 approximation. The program assumes data is available for either a fine group width or a coarse group width of some integer multiple of fine group widths or both. The data required for individual fine groups are the capture and fission cross sections from the resolved resonance calculation, and the elastic transfer and transport cross sections for the materials that are treated in the ELMOE manner. All other data are specified for coarse groups. The output of the routine is both the fine, and coarse group flux.

The central driver for the master program has been written from the beginning of the code to the end of the calculation of the weighting spectrum. This routine starts with the users input specification and calls in the various subroutines to obtain the desired cross section set.

A section has been written to use the present ELMOE library of Legendre coefficients. The number of groups which may be used in the calculation of the weighting spectrum is almost arbitrary since the program is set up to do the calculation in segments. Elastic matrices are read in for each new segment. The inelastic and elastic source from the higher energies is retained in the fast memory.

e. Reactor Physics for High Temperature System

(1) Multigroup Constants. New multigroup constants have been generated for tungsten consistent with the 16-group structure adopted by Hanson and Roach.[6] The recent high energy data by Smith, which were found to be consistent with some previous measurements by Langsdorf, were utilized. Limited tests of these constants against integral criticality measurements show slight improvements in agreement between theory and experiment. Perhaps the most important difference between the new and previously utilized constants is the softer spectral prediction. This is, of course, attributed to the fairly high inelastic cross section measurements and is expected to improve agreement between theory and experiment on such parameters as the prompt neutron lifetime and the $\sigma_f^{U^{238}}/\sigma_f^{U^{235}}$ ratio.

(2) Kinetic Analyses. The near and super-prompt critical behavior of fast neutron core systems surrounded by a light element reflector is under way. These systems are neutronically very similar to the extensively studied fast-thermal systems. The majority of the fissions are fast. A few percent thermal and epithermal fissions are adequate to provide a long (5-25 μsec) neutron lifetime.

The sub-prompt critical kinetics are, as expected, very similar to those of fast neutron systems with heavy metal reflectors and depend only upon the effective shutdown coefficient. The super-prompt critical studies show that a system with a light metal reflector, and a corresponding power spike near the core-reflector interface, behaves somewhat differently from the extensively studied fast neutron systems. Detailed calculations utilized the AX-I program with 4 energy groups. In general, it was found that the long-lifetime systems produced lower peak pressures and kinetic energies than similar fast neutron systems with similar initial reactivity insertions. These conclusions are in essential agreement with very general studies previously reported by Jankus.[7] To date, the most interesting result found in these analyses is the time behavior of the inverse period describing a super-prompt critical excursion. Once the system kinetic energy becomes significant, the inverse period does not always decrease monotonically until the burst is complete.

[6] G. E. Hanson, W. H. Roach, "Six and Sixteen Group Constants for Fast and Intermediate Critical Assemblies," LAMS-2543 (1961).

[7] V. Z. Jankus, "A Theoretical Study of Destructive Nuclear Bursts in Fast Power Reactors," ANL-6512 (1962).

B. Reactor Fuels Development

1. Corrosion Studies

a. Zirconium Alloys for Superheated Steam. The exposure at 650°C of steam-resistant zirconium alloys to flowing steam containing additions of hydrogen and oxygen gas (described in previous reports) is in progress. After 2 weeks exposure, weight gains and appearances were essentially the same as in previous tests without oxygen and hydrogen additions.

Further attention has been given to the chemical and metallographic analysis of samples of the steam-resistant alloys after extensive corrosion at 560°C and 650°C in steam. Micrographs at 250X revealed complex layer structures in both the corrosion films and adjacent metal. In the 650°C samples apparent cracks extended into the unconverted metal from the film-metal interface. In the 540°C samples cracks were observed only in the film. The results of a series of oxygen analyses of as-cast, hot-rolled, and corroded samples of these materials indicate: 1) An oxygen content of about 0.14 w/o in the as-cast materials, 2) little oxygen pickup during hot rolling, and 3) lack of an obvious correlation between alloy composition and amount of oxygen absorbed by bulk metal during corrosion. Microhardness traverses, to be made of the metallography specimens, may yield more information about oxygen absorption and distribution near corroded surfaces.

The hydrogen absorption by samples of these materials corroding in steam has been described. The reason for lower absorption at higher temperature has been considered in terms of an electrical effect associated with thermionic emission at the test temperatures (among other possibilities). Recently an attempt was made to observe the behavior of the potential of corroding Zr alloy with respect to its immediate surroundings. A corroded sample of Zr-Cu-Fe alloy was placed parallel to a plate of Pt in a water vapor environment of about 1 Torr pressure, the minimum plate spacing being 50 microns. As the temperature was raised, the Zr-Pt potential was observed on an electrometer to reverse its sign from Zr-negative to Zr-positive at approximately 600°C. The behavior of these potentials is complex when pressure or temperature is cycled or when the Pt is allowed to touch the corrosion film. Some further study is being made, and at present these findings are to be considered tentative; and whether these findings may be related to corrosion phenomena at 600 psi is still to be established.

b. Ferrous Alloys in Superheated Steam. The dynamic-test facility is now being used for a longer test of Types 304 and 406 stainless steel in 650°C steam flowing at 65 m/sec. Direct additions are made of 30 ppm O_2 and a stoichiometric amount of hydrogen. There is evidence that some recombination occurs in one pass through the facility since the condensate typically runs lower in oxygen (20 ppm) when the hydrogen flow is started.

As with the other tests, the pressure is 0.42 kg/mm^2. To date only data up to 21 days exposure are available, but these indicate no significant difference from earlier tests with oxygen alone.

A refreshed autoclave test of the 304 and 406 stainless steels is being operated at 600°C, 0.42 kg/mm^2. Data for 304 up to exposures of 43 days indicate less than half the corrosion rate found at 650°C. Type 406 appears to corrode to a depth of about 3 x 10^{-4} cm rapidly and then no measurable additional corrosion occurs. This is similar to 650°C experience with this alloy.

c. Protection of Refractory Metals in Liquid Alkali Metals Containing Oxygen. The corrosion behavior of some refractory metals in liquid lithium, sodium, or potassium has been under investigation at many different places. Studies initiated in this Laboratory include: a) the survey of thermodynamic and electrochemical conditions for metal reactions in low oxygen-content liquid metals, and b) the protection of materials in question by reversing the oxidation reactions under appropriate current density conditions.

An experimental cell has been designed and constructed. The measuring and recording circuits have been assembled, tested, and subsequently used for determining the electrical resistance of a liquid-sodium-containing cell. Preliminary runs on Zircaloy-2 samples have indicated that partial oxidation protection has been effected by the employment of about 5 amps/cm^2 in the experimental cell.

d. Light Alloy Suitable for Use with Mercury at Elevated Temperatures. One of the useful methods of retarding corrosion by liquid metals is the addition of metallic inhibitors. It has been repeatedly demonstrated that certain metallic additives which are soluble in the liquid at the temperatures of interest and are not of the same chemical type as the liquid can effectively retard the attack of the liquid on solid structural metals. There has been a general acceptance of the practical and theoretical importance of this approach; however, little work has been done to develop and to understand these systems.

It was previously reported that a saturated solution of aluminum, zirconium, or nickel in mercury resulted in inhibition of the corrosion of titanium at 538°C (1,000°F) for a period of 14 days. Among these additives nickel received more attention because it produced a more effective diffusion barrier layer.

Long-term exposure of titanium to nickel - inhibited at 538°C (1,000°F) for 30, 60, and 90 days - resulted in a consistent sample weight gain with time of exposure (+5.20, +7.81, and +8.90 mg/cm^2 respectively). The newly formed surface layer showed a continuous single phase

after 30 and 60 days and two distinct layers after 90 days. No interface attack under these layers was detected. The weight gain versus time curve showed a decrease in slope between 60 and 90 days.

Work is now proceeding to identify the composition and structure of the nickel-containing protective layer. A loop test is being conducted to investigate the possibility of nickel inhibition in a dynamic system. Experience gained from these tests is expected to be applicable to other liquid metal corrosion problems.

The use of magnesium as a wetting agent in a mercury-steel system is well known. However, a small amount of magnesium (50 ppm) added to the nickel-saturated solution of mercury caused an accelerated corrosion attack on titanium after a 14-day exposure at 538°C (-32.6 mg/cm^2).

e. Aluminum Powder Products. Corrosion tests on aluminum powder product samples are being terminated this month. A final report will be written.

2. Ceramic Fuels

a. Uranium, Thorium, Plutonium Phosphides. The objective of this study is to characterize the compounds in the above phosphide systems and to evaluate their potential as reactor fuel materials. Uranium monophosphide is presently being synthesized by reaction of uranium with phosphine gas.

Electrical resistivity measurements have been conducted on UP specimens sintered at various temperatures. As was expected, the resistivity decreases with sample density, but the decrease is greater than can be explained solely on the basis of density. Resistivity measurements conducted on a dense specimen between liquid-nitrogen temperature and room temperature show a positive linear temperature resistivity relationship in that range. The room-temperature electrical resistivity value is 325×10^{-6} ohm-cm and the temperature coefficient of resistivity is 0.35×10^{-6} ohm-cm/°K.

The UP reacts with metallic uranium to form an anion-deficient structure. At 1600°C, up to 5% of uranium is taken up by the stoichiometric phosphide. The unit cell contracts as the composition departs from stoichiometry. Stoichiometric UP has a lattice constant of 5.589 Å, while the composition $UP_{0.95}$ has a value of 5.582 Å. Based on these preliminary results and assuming a linear relationship of lattice constant to composition, a composition in the vicinity of $UP_{0.86}$ exists at or around the melting temperature (2730°C). This composition results from the preferential loss of phosphorus from the structure. The range of solid solution of uranium in UP will be further determined at temperatures higher than 1600°C.

3. Fuel Jacket Development for High Temperature Applications

In an effort to produce thin-walled small-diameter tungsten tubing, some encouraging results have been achieved.

A 0.250 in. OD x 0.205 in. ID vapor-deposited tungsten sleeve with a molybdenum core was jacketed in Type 304 stainless steel. The assembled billet was extruded at 1250°C at a 4.2:1 extrusion ratio. The stainless steel was removed by machining the aqua-regia dissolution while the molybdenum core was etched away by a 30 to 60% HNO_3 solution. The dimensions of the extruded tube were 0.124 to 0.128 in. OD x 0.011 to 0.012 in. wall thickness. (Ovality present in the starting sleeve was not removed by extrusion.) The surface of the extruded tube was good and metallographic examination revealed a typical worked structure.

4. Irradiation Studies

a. Irradiation of Thorium-Uranium Alloys. A group of 44 thorium-uranium alloy castings containing 10, 15, 20, 25, and 31 w/o uranium irradiated to burnups up to 10 a/o were found to show unusually good resistance to high temperature swelling (ANL-5674). Electron microscopy is being performed on some of the irradiated specimens in order to determine the reasons for their excellent dimensional stability under high-temperature irradiation and postirradiation annealing.

The initial examination of a Th-10 w/o U alloy specimen irradiated to 4.0 a/o burnup at 560°C shows that a dispersion of approximately 3.1×10^{12} particles of uranium per cm^3 of fuel alloy was obtained. Small pores about 0.1μ in diameter were present and were attributed to fission gas bubbles. The bubbles were almost without exception attached to second phase uranium particles.

5. Extrusion Development

Attempts to extrude molybdenum tubing at 1100°C by the modified DPM technique were unsuccessful. Billets were rapidly heated in air by an induction coil. Examination of a billet that only partially extruded (approximately 10%) yielded interesting information. The wrought molybdenum sleeve exhibited a fully recrystallized structure in the unextruded portion resulting from induction heating. The molybdenum core (insulated from the sleeve by the powder annulus) showed no evidence of recrystallization. Since induction heating generates heat near the surface of the work piece, the insulated central molybdenum core received little if any heat during the short heating time and prevented complete extrusion of the billet.

6. Nondestructive Testing

a. Neutron Imaging. Neutron radiographic inspections completed this month include 24 clad plutonium fuel pins, and 5 pressed uranium oxide cylinders radiographed both individually and after assembly into a stainless steel container.

No flaws were detected in the UO_2 material but several of the plutonium fuel pins appeared to contain suspect, high-transmission areas.

b. Ultrasonic Imaging. The continuously-pumped ultrasonic imaging system at ANL is being used to determine some of the resolution characteristics of the system. Under good conditions the useful depth of focus of the imaging system may be in the range 7.62 cm to 10.16 cm, a distance somewhat greater than anticipated; but the object-detector distance for useful image-resolution is showing extreme dependence on ultrasonic frequency.

c. Application of Infrared Radiation to Nondestructive Testing. Investigation of the possible use of infrared in nondestructive testing has continued. Some attempts to improve the temperature and angular resolution of the infrared scanning system have been made. However, it has been demonstrated that this system in its present form is not as sensitive to surface temperature differences as the thermographic phosphor when applied directly to the surface of the test object. By placing the test object in an ice bath and applying heat to the phosphor coated surface, steady state temperature differences can be maintained on the surface over artificially produced defects. These temperature differences cannot be imaged with the scanning system.

C. Reactor Materials Development

1. Structural Materials

a. Brittle Fracture Studies. Preparation of an Amsler-Schnadt Impact Testing Pendulum for making Charpy V-notch and Schnadt coheracy tests is almost complete. Final alignment between the striker and specimen was established by machining the anvils approximately 0.020 in. This allowed the anvils in the base of the machine to be adjusted sideways so that the specimen can be positioned centrally with respect to the striker.

Leaf springs were mounted on the anvils to permit positioning the specimen in the machine accurately with a minimum of effort. The energy absorbed in the springs during fracture of the specimen was computed to be insignificantly small - of the order of 0.1 ft-lb. A thermocouple attached to one of the springs makes contact with the end of the specimen. The temperature of the notch can be determined from a calibration curve.

Figure 10 shows the notch temperature T_N as a function of the end temperature T_E. Specimens are brought to temperature by soaking in a heated or cooled bath, and the exact test temperature (T_N) is obtained by reading the end thermocouple and using Figure 10.

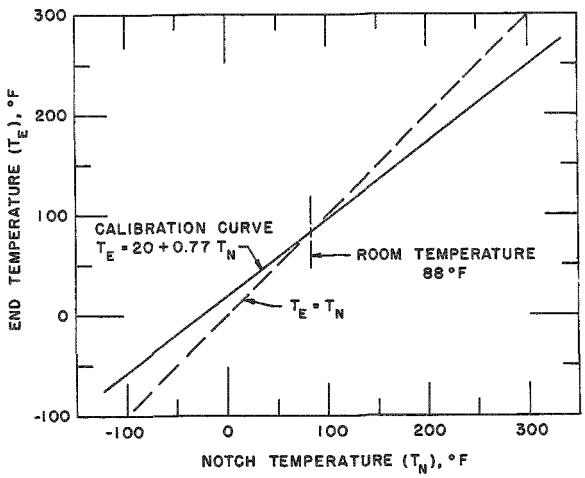

Figure 10

Calibration Curve for Determining Temperature of Notch from Temperature Measurement Made on the End of the Charpy Specimen. The dashed line would apply if no temperature gradient existed between the notch and the end of the specimen.

The behavior of the broken specimen was studied using high speed photography. So far, seven films have been taken of specimens broken under various conditions. It is hoped that the results will aid in understanding the factors which contribute to the scatter in impact testing data.

b. Development of Fast Neutron Monitoring Techniques. A study has been undertaken by H. Moret, Central Bureau of Nuclear Measurements, Geel, Belgium, to use the density change of a quartz crystal to monitor fast neutron flux. Nine quartz crystals have been obtained from Moret for irradiation in the CP-5 reactor. They will be returned for analysis in a special density gradient column capable of measuring density accurately to 5×10^{-5} gm/cm^3.

The literature on radiation effects on the structure of quartz has been reviewed. It appears that measurable density changes occur at exposures of the order of 10^{19} n_f/cm^2. Irradiation temperature is not an important variable.

Density changes in quartz, however, are not a simple linear function of integrated exposure. In addition, density changes are also associated with a loss of crystalline order with sufficient exposure. The crystalline structure changes to an amorphous form similar to that of vitreous silica.

D. Heat Engineering

1. Two-phase Critical Flow for Liquid-Metal Systems

Existing data and models for critical two-phase flow of steam water have been examined critically. One model in particular has shown considerable success in predicting the critical flow phenomena (see ANL-6633). This model has been utilized to predict void fraction, slip ratio, and critical flow rates for various liquid-vapor metal systems in pipes when the conditions are such that critical flow may be experienced. The following liquid-metal systems have been calculated: mercury (temperature range 450-1600°F), cesium (temperature range 500-2300°F), rubidium (temperature range 500-2300°F), potassium (temperature range 900-2500°F), sodium (temperature range 950-2500°F), lithium (temperature range 2000-3500°F). The vapor fraction or quality ranges from 0 to 100 percent.

Critical flow rates for liquid-metal systems calculated from the best model describing steam-water data, are considerably higher in the low-quality region than predicted from a so-called "Homogeneous Flow Model." This is explained by the large slippage between the liquid and the vapor phases because the ratio of the densities of the liquid state to the vapor state is usually large for metallic fluids.

A report is in preparation describing these results.

2. Simulation of Two-phase Heat Transfer with Gas Injection through a Porous Boundary Surface

Hydrodynamic aspects of two-phase boiling heat transfer are being investigated in this study with an analogous, two-component system, where gas is injected through a porous surface into the liquid at the solid-liquid interface. Previous analytical studies by several investigators have shown that this system simulates the hydrodynamic effects of boiling quite well theoretically, and that the initial and boundary conditions are the same.

For this study, the effort is concentrated on the investigation of the forced circulation boiling heat transfer, because this type of system is of great interest and importance in the reactor engineering field. The experimental loop is constructed using a vertical porous tube in which only the upper portion is heated. Water is pumped through the center of the tube and the air is injected radially into the tube. A transparent exit section is used to observe flow patterns. This arrangement and system offers advantages in studying boiling because gas evolution rate, mass flow rate, and gas quality are controlled independently. Therefore, the hydrodynamic aspects of boiling can be studied at low temperatures for a wide range of conditions.

To date, the experimental investigations performed with this loop include studies of the void fraction of air-water mixtures using gamma attenuation techniques, and a number of air-water heat transfer studies.

The void fraction study was performed because it is believed that void fraction and radial phase distribution are important parameters strongly affecting the heat transfer coefficient. The results of this study for air-water mixtures indicated that the relative velocity of the two phases is strongly influenced by wall air injection rate and incoming liquid velocity. Radial phase distributions in the pipe were determined from gamma attenuation measurements to illustrate and help explain the injection effects. When these results are compared to void fraction and void profile results of systems where there is no injection or "nucleation" at the wall, appreciable differences can be noted, which point out the importance of nucleation (or injection) at the wall in determining the hydrodynamic and heat transfer conditions in two-phase boiling systems.

The results of the air-water heat transfer experiments analyzed to date show that the effect of gas injection and the gas phase on the heat transfer coefficient is much more pronounced at lower liquid mass flow rates, and becomes smaller as the mass flow rate increases. For instance, the two-phase heat transfer coefficient is more than three times the liquid heat transfer coefficient at liquid mass flow rates at Reynolds number of 10,000, and goes down to 1.3 times at Reynolds number of 50,000.

When gas injection is increased at a constant phase ratio and liquid mass velocity, the initial injection increases the heat transfer coefficient substantially, but additional increases in injection do not add much to it. If gas injection through the wall is increased to very high rates, it even begins interfering with heat transfer, because the liquid is partly removed from the heat transfer surface. The interference is more pronounced at higher liquid mass flow rates, where the gas tends to stay closer to the heating surface as radial phase distribution profiles at the test section indicate.

Flow patterns were found to have an important effect on heat transfer. Gas injection was found to contribute a substantial portion of the large increase in heat transfer coefficient when flow changed from single-phase liquid to the bubbly flow (two-phase) regime. The heat transfer coefficient did not change substantially in the slug flow (large bubbles) region, and increased steadily in the annular flow region. However, in the annular flow region, injection was beneficial in increasing heat transfer only at low liquid mass flow rates, and actually interfered with it at higher mass flow rates.

3. Thermodynamic Properties of Pu^{239} as an Ideal Gas

The entropy, enthalpy, specific heat, and free energy in the temperature range 298.15°K to 5000°K were calculated for Pu^{239} as an ideal monatomic gas based on Gerstenkorn's recently published analysis of the optical spectrum of Pu^{239}. To perform the calculations, an IBM-704 program was devised, which evaluates thermodynamic functions from spectroscopic data by means of the partition function.

4. Boiling Liquid Metal Studies

Design is completed for a small-scale boiling liquid metal experiment. Assembly of the loop is now in progress. The Type 316 stainless steel loop has a 10-kw radiant heated section and a coil condenser. The coil is designed to remove 10 kw by radiation heat transfer when the liquid metal is at 1500°F. Initially NaK will be used as the heat transfer fluid.

5. Measurement of the Vapor Pressure of NaK

Measurements of the vapor pressure of NaK up to pressures of 25 atm have recently been completed. It was shown that the vapor pressure is a linear function of log P and that the values lie between those of pure potassium and sodium. In addition, it was found that particular compositions of NaK do not have a fixed boiling point since a certain composition will commence boiling at one temperature and continue to boil with a steadily changing composition over a 40°C temperature range. Azeotropic plateaus were not observed. The measured vapor pressures are slightly below those predicted from Raoult's Law indicating that weak intermolecular forces are present.

E. Chemical Separations

1. Chemistry of Liquid Metals

a. Plutonium-Cadmium Galvanic Cell Studies. The investigation of the thermodynamics of the plutonium-cadmium system by means of galvanic cells continues. A second cell has been constructed which has the configuration

Pu-Cd (two-phase alloy)/$PuCl_3$, KCl-LiCl/Pu-Cd (liquid phase)

The second cell differs from the first cell used (see Progress Report for May 1963, ANL-6739, page 49) in that two alloy electrodes are employed in the second cell whereas a pure plutonium electrode and one alloy electrode are used in the first cell. The data obtained with the two cells over the temperature range of 693 to 887°K are in excellent agreement. The new cell with the two alloy electrodes may permit measurement of thermodynamic properties of the plutonium-cadmium system above the melting point of plutonium.

b. Study of Rare Earth-Cadmium System by the Effusion Balance Method. The effusion method is being used to investigate the intermetallic phases and thermodynamic properties of the rare earth-cadmium systems. Studies of the holmium-cadmium system indicated the presence of the following phases: $HoCd_6$, Ho_3Cd_{13}, $HoCd_2$, and HoCd. Studies of the thulium-cadmium system indicated the presence of $TmCd_6$, Tm_3Cd_{13}, $TmCd_2$, and TmCd.

2. Uranium Oxide Reactions in Molten Halides

The likelihood that UO_2Cl thermally decomposes in the ternary eutectic, sodium chloride-potassium chloride-magnesium chloride, to form uranium dioxide and chlorine was reported earlier (see Progress Report for June 1963, ANL-6749, page 42). It has since been demonstrated that this decomposition occurs under vacuum at temperatures above 700°C. Solid material separated from the salt by filtration has been identified as uranium dioxide by X-ray diffraction.

3. Liquid Metal Distillation

Vaporization from the liquid-vapor surface of a liquid pool without the formation of vapor bubbles (nonturbulent vaporization) is essentially an entrainment-free method of vaporization. It therefore may be useful in certain steps of pyrometallurgical recovery processes, for example, in boiling down the plutonium-magnesium-zinc product solution of the blanket process. In the most recent work, a pool of mercury $2\frac{5}{8}$ inches in diameter and 3 inches deep was induction-heated with 10 kc power. During the nonturbulent vaporization of the mercury at low pressure (<1 mm Hg), vertical traverses of the pool centerline with a special thermocouple revealed a steep temperature gradient of about 10°C through a narrow zone (~0.16 inch thick) at the vaporizing surface. Below this layer, the temperature of about 185°C was almost constant. Conductive heat transfer based on the gradient of 10°C accounts for only about 10 percent of the vaporization rate. The remainder of the necessary heat transfer appears to be by convection.

4. Fluidization and Volatility Separations Processes

a. Decomposition of PuF_6 by Gamma Rays. The gamma decomposition of plutonium hexafluoride to plutonium tetrafluoride and fluorine in the presence of krypton is being investigated. In previously reported experiments made with krypton at average krypton electron fractions between 0.08 and 0.91 and with an absorbed energy in plutonium hexafluoride alone of about 15×10^{20} ev (see Progress Report, May 1963, ANL-6739, page 51), the krypton produced a complex effect on the decomposition of plutonium hexafluoride which appeared to depend upon the electron fraction of krypton in the mixture of plutonium hexafluoride and krypton. In current experiments made with krypton at average krypton electron fractions between

0.15 and 0.83 and with an absorbed energy in plutonium hexafluoride alone of about 30 x 10^{20} ev, the krypton produced a similar complex effect on the plutonium hexafluoride. In Figure 11 G-values for the decomposition of plutonium hexafluoride samples (about 80 mm Hg) are plotted against the electron fractions of krypton in the mixtures. It is seen that the G-values fall from an initial value of 7.5 in the absence of krypton to a minimum of about 4.3 at an electron fraction of krypton of about 0.15. The G-value then rises to a maximum value of approximately 6.5 at an electron fraction of krypton of about 0.28 and then falls gradually to zero at an electron fraction of krypton of one. Additional experiments are planned which will investigate the krypton electron fraction region from 0.1 to 0.3.

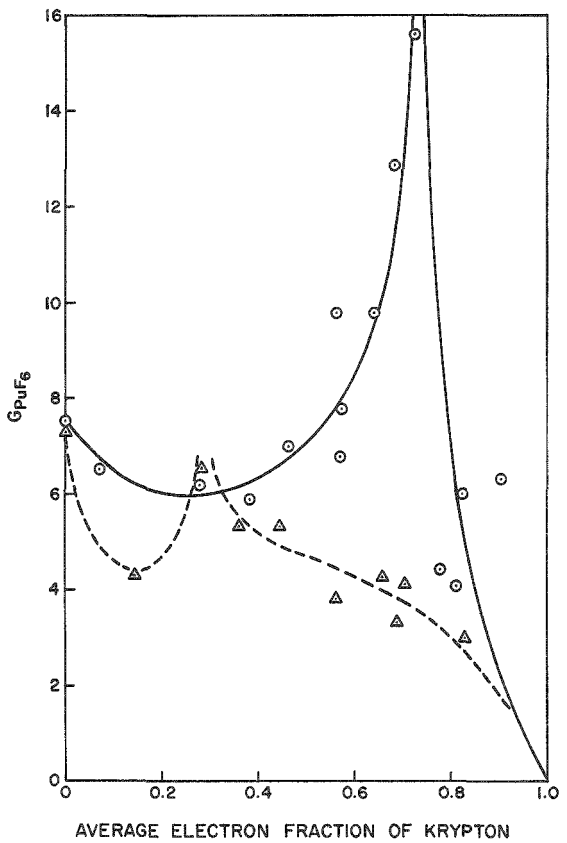

Figure 11
Effect of Krypton on Decomposition of Plutonium Hexafluoride

Exposure Dose
(absorbed energy in PuF_6 only)

O ~ 15 x 10^{20} ev

Δ ~ 30 x 10^{20} ev

PuF_6 sample 80 mm Hg G value - molecules PuF_6 decomposed per 100 ev of absorbed radiation

b. Fluid-Bed Fluorinations of U_3O_8-PuO_2 Mixtures. Laboratory development work is now being directed toward the study of fluid-bed fluorinations. Studies of the fluorination of mixtures of plutonium dioxide in uranosic oxide in the presence of Alundum are being made in a $1\frac{1}{2}$-inch diameter reactor (see Progress Report, June 1963, ANL-6749, page 43). The feed material (PuO_2-U_3O_8 mixture with Alundum) is fed to the fluidizing gas (nitrogen) which also serves to transport the feed material to the fluid-bed fluorinator reactor. The results of these studies will be used to establish the optimum conditions for the formation and removal of uranium and plutonium hexafluorides.

In four experiments, the fluorinations were carried out in two steps. The first step was a feeding-fluorination period (1 hr) during which the feed material (300 g PuO_2-UO_2; 150 g Alundum) was transported into the fluid-bed reactor and simultaneously reacted with fluorine (20 v/o fluorine in nitrogen once-through gas flow) at a bed temperature of 500°C. The second step, which immediately followed the feeding-fluorination period, was an additional fluorination period (5 hr) using total off-gas recycle with fluorine at a concentration of 100 percent. The second fluorination was carried out at a bed temperature of either 500°C or 550°C. The PuO_2-U_3O_8 mixtures (0.35 w/o plutonium; 84.19 w/o uranium) for these experiments were prepared by blending uranosic oxide (325 mesh) with the products of the air oxidation of PuO_2-UO_2 solid solutions. A 120 mesh Alundum was used in the feed and for the fluidized bed (400 g) in the fluorinator reactor. The operating conditions and the results of these runs are summarized in Table X. The residual plutonium content of the Alundum varied from 0.018 to 0.063 w/o in these fluid bed runs. This compares favorably with the residual plutonium value of 0.007 w/o obtained in the boat-type fluorination experiments which were carried out at similar temperatures for 20 hr (see Progress Report, August 1962, ANL-6610, page 55). Additional experiments are planned in which reaction conditions will be modified to achieve improved recovery of plutonium.

Table X. Summary of Operating Conditions and Results of Fluid-Bed Fluorinations of PuO_2-U_3O_8 Mixtures

Feed Charge: 300 g PuO_2-U_3O_8; 150 g Alundum
Reactor Bed: 400 g Alundum
Reaction Conditions: (1) Feeding-Fluorination Period - Bed Temperature: 500°C; 1 hr; 20 v/o F_2, 80 v/o N_2

(2) Recycle-Fluorination Period - Bed Temperature: 500°C (Runs UP-1, UP-2) or 550°C (Runs UP-3, UP-4); 5 hr; 100 v/o F_2

	Residue (w/o)[a]		Conversion to Hexafluoride (%)	
Run No.	Plutonium	Uranium	Plutonium[b]	Uranium[c]
UP-1	0.033	0.0212	82.1	99.95
UP-2	0.063	0.0045	65.6	99.97
UP-3	0.022	0.0027	88,2	99.99
UP-4	0.018	0.0096	90.1	99.96

[a]Retained by Alundum bed.

[b]Plutonium dioxide to plutonium hexafluoride.

[c]Uranosic oxide to uranium hexafluoride.

c. Oxidation-Fluorination Reaction of Clad Uranium Dioxide Pellets in a Single Reactor. The development of a fluid-bed oxidation-fluorination scheme for the processing of stainless steel-clad uranium dioxide pellets in a single reactor is continuing in engineering-scale runs. In this scheme, there are two distinct reaction zones: the first is a bed of uranium dioxide pellets with Alundum particles in the voids (oxidation zone); the second is a bed of Alundum particles placed over the uranium dioxide pellet bed (fluorination zone). In the oxidation zone, U_3O_8 fines are produced by contacting the uranium dioxide pellets with an oxygen-nitrogen stream which also serves to fluidize the Alundum particles. The U_3O_8 fines are elutriated from the lower zone by the oxygen-nitrogen gas stream and are reacted in the upper zone with fluorine, which is admitted to the fluidized bed of Alundum just above the uranium dioxide pellet bed. The fluidized Alundum serves as a heat transfer medium.

A run was made which continued the evaluation of the effectiveness of the two-zone oxidation-fluorination scheme for the removal of uranium dioxide from stainless steel cladding (see Progress Report, June 1963, ANL-6749, page 44). To simulate sheared pieces of clad fuel elements, about 1-in. long by $\frac{1}{2}$-in. diameter stainless steel cladding with the ends left open was used to contain uranium dioxide pellets. The wall thickness of the cladding was 0.020 in.

In this run, a 3-in. deep static bed of clad uranium dioxide pellets (1.7 kg uranium dioxide) and a 17-in. deep fluidized Alundum zone (6.1 kg) were used. The Alundum (120 mesh commercial grade) used in this run was screened to remove the fines (-200 mesh) in order to improve solids mixing. The charge consisted of 85 fuel segments (2 UO_2 pellets in each segment). The following operating conditions were used in this run. In the oxidation zone, the composition of the fluidizing gas was 88 percent oxygen in nitrogen at a total gas flow rate of 0.3 cu ft/min. In the fluorination zone, the concentration of the fluorine in the gas mixture was from 3 to 14 percent (dilution of the fluorine was obtained by recycling the process off-gas at a rate of 0.65 cu ft/min). The temperature in the oxidation zone was maintained at 400°C for 8.5 hr and then at 500°C for 3.5 hr. The temperature in the fluorination zone was 500°C. Gas pulsing of the fluidizing gases was used. The pulse duration was 0.04 sec. with a pulse frequency of 2 pulses/min at a gas manifold pressure of 20 psig. About 87 percent of the uranium dioxide was removed in a processing time of 12 hr (once-through gas flow). The fluorine utilization efficiency was 42 percent. The run was then continued (single-zone fluorination operation in which the fluorine is introduced at the bottom of the reactor) for an additional period (5 hr) of total off-gas recycle with fluorine added to a maximum concentration of 64 percent for further uranium removal. This resulted in additional removal of uranium for an overall uranium removal of greater than 99.9 percent (based on the uranium oxide residue remaining with the cladding).

d. Decladding of Fuel Elements by Fluid-bed Oxidation. Separate studies are being made to find improved methods for the removal of uranium dioxide pellets from stainless steel cladding by oxidation of uranium dioxide to uranosic oxide in a fluidized bed. Removal of the cladding depends on the conversion of the dioxide to U_3O_8, which creates large internal stresses within the uranium dioxide pellets because of the difference in densities of the two oxides and results in the fragmentation of the pellets. The U_3O_8 fines that are formed in the reaction are elutriated from the pellet bed (oxidation zone) into the fluorination zone of the reactor by the oxidizing gas stream.

Three engineering-scale runs were made to evaluate internal vibration of a packed-fluidized column as a means of assuring the motion of clad uranium dioxide pellets. Vibratory motion of the clad pellets would aid in loosening residues of uranosic oxide which may become wedged in the cladding as a result of the change in density during the oxidation reaction. Internal vibration was obtained by mounting a magnetic vibrator at the bottom of the reactor. This type of vibration is considered preferable to external vibration (see Progress Report, June 1963, ANL-6749, page 45) because the power from internal vibration is applied directly to the bed, and stresses in the reactor are minimized.

In the three runs, the fuel charge consisted of 1-in. long by $\frac{1}{2}$-in. diameter stainless cladding containing uranium dioxide. The ends of the cladding were open to simulate sheared fuel elements. A total packed-fluidized bed height of about 15 inches (static) and a clad pellet bed height of 6 inches (0.81 kg uranium dioxide) were used. Gas pulsing of the fluidizing gas was used; the pulse duration was 0.5 sec. with a pulse frequency of 2 pulses/min at a gas manifold pressure of 30 psig. The reactions were carried out in a 2-in. diameter fluidized-bed reactor.

In two of the runs, the uranium dioxide was oxidized with air, reduced with hydrogen (5 v/o hydrogen in nitrogen), and then reoxidized with air. In these runs, the oxidation and reoxidation temperatures were 450°C, and the hydrogen reduction temperature was 600°C. In the first run, nitrogen was used as the fluidizing gas during the heating-up period. About 93 percent of uranium was removed from the fuel segments charged in a reaction time of 12.3 hr. Uranosic oxide residues were mostly found in the fuel segments located near the bottom of the reactor. The internal vibration was apparently not as effective near the bottom of the bed as in the other parts of the bed. In the second run, air was used as the fluidizing gas (instead of nitrogen) during the heating-up period. Also, a 1-inch deep layer of short lengths of stainless steel tubing was placed on the support plate to serve as a bed support for the fuel segments in order to improve the removal of uranium oxide residues in this portion of the reactor bed. About 96 percent of the uranium dioxide was removed from the fuel segments charged during a reaction time of 11.5 hr.

In the third run, the uranium dioxide was only oxidized, that is, reduction with hydrogen and reoxidation with air were not carried out. The oxidation reaction temperature was slowly increased to 450°C. Air was used as the fluidizing gas during the heating-up period. About 99 percent of the uranium dioxide was removed from the fuel segments charged in a reaction time of 8.7 hr.

The results of these runs indicate that a uranium dioxide separation of 99 percent can be achieved by slowly increasing the oxidation reaction temperature to 450°C and utilizing gas pulsing and internal vibration of the packed bed. The use of additional reduction and reoxidation treatment does not appear to be necessary.

e. Separation of Uranium from Zirconium Alloy Fuels. The development of a chlorination-fluorination scheme for reprocessing highly enriched uranium-zirconium fuels was continued. In the present scheme, the fuel is first reacted with hydrogen chloride in a fluidized bed of inert solids. This reaction converts the zirconium to the tetrachloride and the uranium to the trichloride. Since the hydrochlorination step is carried out at temperatures above the sublimation point of zirconium tetrachloride (331°C at 1 atm), a separation of the zirconium tetrachloride from the solid uranium trichloride is achieved. The uranium trichloride is then converted to the volatile uranium hexafluoride by reaction with fluorine and is thereby removed from the inert solids of the fluidized bed.

In current work, the disposition of the minor constituents of Zircaloy-2 during the entire reaction cycle was determined as a preliminary step towards establishing the distribution of fission products. The disposition of the constituents of Zircaloy-2 were based on the results of analyses of samples (for a number of runs) taken from the reaction beds and zirconium tetrachloride condenser. These runs have included reaction cycles in which the hydrochlorination step (dry hydrogen chloride) was carried out at temperatures between 350 and 500°C and the fluorination step was carried out at temperatures between 250 and 500°C.

The distribution of the minor constituents of Zircaloy-2 was found experimentally to be in conformity with the distribution estimated from the volatilities of their higher valent chlorides and fluorides. Tin and iron (as stannic chloride and ferric chloride) volatilized together with zirconium tetrachloride throughout the hydrochlorination step. Hafnium and titanium as well as aluminum, boron, beryllium, cadmium, lead, rubidium and silicon were volatilized during the hydrochlorination step. Chromium was retained by Alundum in the fluid bed during the hydrochlorination step, but was volatilized during the fluorination step. Magnesium, calcium, strontium and barium were retained by Alundum in the fluidized bed throughout the entire reaction cycle.

In order to simplify the treatment of excess hydrogen chloride, hydrogen fluoride, and fluorine in the process off-gas, dry disposal methods are being investigated. Soda lime is being tested for the treatment of hydrogen chloride and hydrogen fluoride; and, a mixture of salt and soda lime for fluorine. In preliminary tests for the disposal of hydrogen chloride or hydrogen fluoride with soda lime, reaction efficiencies of greater than 99 percent were indicated. Tests for the disposal of fluorine using a mixture of salt and soda lime are now underway.

5. General Chemistry and Engineering

a. Conversion of Uranium Hexafluoride to Uranium Dioxide: Preparation of High-Density Particles. Development of a fluid-bed method for producing high-density spheroidal uranium dioxide particles by the simultaneous reaction of uranium hexafluoride with a mixture of steam and hydrogen has been continued. The reactions have been carried out in the temperature region from 650 to 700°C. Uranium dioxide with particle densities of up to 89 percent of theoretical have been produced directly at 700°C; final particle densities of 96.5 percent of theoretical were obtained by sintering in hydrogen at 1725°C. The dense uranium dioxide particles would be intended for use in dispersion fuels or in bulk form in packed fuel elements.

In current work, the effect of increased uranium hexafluoride feed rate (from 25 g/min to 50 g/min) on the properties of the uranium dioxide particles formed was studied. The run was made in which the following operating conditions were used. Thirty-minute uranium hexafluoride-feed periods, in which 50 g uranium hexafluoride/min was reacted with steam and hydrogen at rates equivalent to 1.3 and 7.3 times the stoichiometric requirement,* respectively, were followed by 30-min cleanup periods to complete the conversion of the uranium hexafluoride to uranium dioxide. During the cleanup periods, only steam and hydrogen were fed. The concentration of steam in this period was increased from 26 to 50 volume percent in order to reduce the residual fluoride content of the product. The reaction temperature was 650°C. The starting bed was composed of uranium dioxide particles which had a density of 9.3 g/cc (-18 +230 mesh size). Seed particles of uranium dioxide (-60 +230 mesh) were added in this run. The filter fines were returned directly to the reactor (see Progress Report, June 1963, ANL-6749, p. 47). The operating period for this run was 12 hr. The particle density of the as-produced uranium dioxide product decreased slightly from the initial value of 9.3 g/cc to 8.8 g/cc during the run period. The increased steam rate during the cleanup period was effective in reducing the residual fluoride content to 0.021 percent (despite the increased uranium hexafluoride feed rate of 50 g/min). Microscopic examination of the product particles showed increased surface roughness which was noted in earlier work (ANL-6023).

*Based on the reaction $UF_6 + 2H_2O + H_2 \rightarrow UO_2 + 6HF$.

b. Preparation of Uranium Monosulfide. Three 100-gram batches of uranium monosulfide, which were prepared by the reaction of hydrided-dehydrided uranium metal with a stoichiometric quantity of hydrogen sulfide and subsequent sintering in vacuum at 1900°C for 2 hr (see Progress Report for June 1963, ANL-6749, page 32), have been analyzed for trace impurities. Nitrogen and carbon contents were found to be about equivalent to those in the uranium metal used for the preparation (0.002 and 0.027 w/o, respectively), and no significant amounts of metallic impurities were introduced into the product. The oxygen contents were high, varying from 0.09 to 0.4 w/o, as compared with 0.0018 w/o oxygen in the starting uranium metal.

c. Thermodynamics of Binary Alkali Metal Solutions. Study of the thermodynamics of binary solutions of the alkali metals by the optical absorption method is continuing (see Progress Report for June 1963, ANL-6749, page 42). Preliminary tests are being made to calibrate the absorptiometer and to evaluate the suitability of different types of absorption cells. In the present study a Kovar cell with sapphire windows is being used. The absorption of sodium at 5890 Å (one of the sodium-D lines) has been measured at several temperatures in the range 180 to 220°C. The temperature dependence of the absorption (which is proportional to the pressure of sodium atoms in the vapor) was used to make a preliminary calculation of the enthalpy of vaporization. The enthalpy of vaporization value thus obtained agrees to within 3 percent with the best literature value. However, additional measurements are required before a more exact treatment of the data can be made.

d. Preparation of Carbides. Reactions between magnesium dicarbide and the oxides of various metals in a molten halide flux have been carried out in an effort to prepare carbides of the metals. Reactions with the oxides of uranium, thorium, titanium, zirconium, and silicon were carried out under vacuum at a maximum temperature of 770°C. A 35 m/o magnesium chloride flux was used as the reaction medium. Sodium tungstate, uranium tetrafluoride, and magnesium uranate were also reacted with magnesium dicarbide. The following carbides have been prepared (although not isolated as pure materials) by the reaction of metal oxides or halides with magnesium carbide in molten chloride media: UC, ZrC, β-SiC, WC, α-W_2C, VC, TaC, Mo_2C, and UC_2. X-ray diffraction was used to identify the carbides.

In another experiment, the solubility of magnesium sesquicarbide in a 35 m/o lithium chloride-65 m/o magnesium chloride flux at 600°C was found to be 1.99 w/o.

F. Plutonium Recycle Program

1. Nondestructive Tests on Components

Test equipment (described in the June Progress Report, ANL-6749, p. 51) was installed in the plant of the Harvey Aluminum Company in

Torrance, California in order to evaluate Zircaloy-2 jacket tubing of nominal OD 10.67 mm and wall 0.686 mm. The system has proved itself reliable and simple enough for operation in a fabricator's plant by semi-skilled personnel, but a faster inspection rate is desirable if it can be obtained without a loss in sensitivity and resolution. A high noise level was obtained from certain tubes containing heavy tube-reducer marks. Extensive metallography on these tubes revealed no significant defects, so it will be necessary to modify the test equipment to eliminate these spurious signals which might otherwise mask real defect signals. This seems possible by stationing an additional sampling pulse at such a point in time of the main reflected pulse that the sampling pulse will be able to obtain information concerning this effect independent of any of the wall defects. This information can then be used to reduce the effect of the variation in the main reflected pulse resulting from the tube reducer marks.

The flaws discovered in the tubing occurred either as shallow surface laps, probably incurred during belt sanding, or as defects appearing along a 45° shear plane containing the tube axis. The longest of the latter defects was about 0.01 mm long. These objects may be cracks which occur at some early stage of the process and are then later partially healed. A good estimate of the incidence of flaws is difficult because of the small sample that was tested, but the rate of defect occurrence seemed relatively low compared to some previous experiences with Zircaloy-2 tubing.

IV. ADVANCED SYSTEMS RESEARCH AND DEVELOPMENT

A. Direct Conversion by Thermionic Emission with a Cesium Cell

The design of a thermionic cell used in certain direct conversion experiments, is described in ANL-6705 (Progress Report for March, 1963). Briefly, the interelectrode distance is held to 1 mm or less and is small compared to the electrode dimensions. In addition, the collector is surrounded by a guard ring. For each test, the cell is operated at a constant cesium vapor temperature of T_0, and a collector electrode temperature, T_C, where usually $T_C = T_0$. The emitter temperature, T_E, however is varied.

The measurement of the saturation values of the cesium ion current at given cesium vapor pressures and concentrations were recently repeated and compared with values obtained by calculation using equations developed here.

The expected saturation current was calculated using the following assumptions:

(1) Equilibrium exists at the boundary of the thermionic cell which includes the emitter-collector so that an equal number of atoms diffuse into and out of the cell.

(2) The mean free ion path (mfp) is large everywhere compared to the emitter collector distance.

(3) Atoms moving between the emitter and collector leave the emitter at T_E and collector at T_C.

(4) A portion "α" of the atoms leaving the emitter are ionized according to the Saha-Langmuir equation and neutralized at the collector.

Assumptions (1) through (4) result in the following expression for the cesium ion current:

$$I_{Cs+} = \alpha n_{Cs}\ 5.045 \times 10^{-14}\ \sqrt{T_0}\ \text{ma} \qquad (1)$$

where

I_{Cs+} = Cesium ion current/cm^2

n_{Cs} = Cesium atom/cc at temperature T_0

ma = milliampere

The atomic and ionic densities between the emitter and collector are given by:

$$n_E = \frac{n_{Cs}}{2}\sqrt{\frac{T_0}{T_E}} \tag{2a}$$

$$n_C = \frac{n_{Cs}}{2}\sqrt{\frac{T_0}{T_C}} \tag{2b}$$

$$n_{Cs+} = \alpha n_E = \alpha \frac{n_{Cs}}{2}\sqrt{\frac{T_0}{T_E}} \tag{3}$$

where

n_E = Atomic density of "hot" atoms + ions

n_C = Atomic density of "cold" atoms

n_{Cs+} = Ion density

A comparison of the calculated and experimental values showed that the experimental results were larger than the calculated values by a factor of 1.5 or 2. It is therefore evident that these differences must be resolved through either improved experimental or calculational techniques.

B. Magnetohydrodynamic Power Generation

1. Variable Area MHD Generator

In the MHD liquid metal direct conversion systems, where the kinetic energy of the high velocity liquid is directly converted to electricity, there is an advantage to increasing the flow area for the liquid as it passes through the magnetic field. As kinetic energy is converted to electrical energy the fluid slows down in the diverging duct. The duct area may be varied in several ways: (1) so the voltage generated is a constant, (2) so the electrical resistance is lower as the fluid slows down in the magnetic field (3) or so that the power removed from the fluid in the duct is a constant. In this generator the area was varied to lower the electrical resistance.

An experimental system has been built in which nitrogen gas is mixed with NaK liquid. After the mixture is accelerated in a nozzle it is passed through the generator duct. Experiments to test the feasibility of the diverging or variable area generator duct were performed.

A variable area generator made of Lucite was fabricated and tested. The dimensions of the generator are:

Inlet dimensions	0.16 cm x 10 cm
Outlet dimensions	0.45 cm x 10 cm
Length of generator through the magnetic field	3.2 cm
Magnetic flux	9000 gauss
External load	
Resistance of load	1×10^{-4} ohm

Several runs were made in which the ratio of NaK to nitrogen gas was varied. Table XI shows the data obtained from the various runs.

Table XI. MHD Variable Area Generator Runs

Run No.	NaK Flowrate cfm*	Gas Flowrate cfm (STP)*	Voltage, Mv	Power, Watts
1	2.16	69.4	17.5	2.96
2	1.75	86.5	20.8	4.34
3	2.73	66.0	25.0	6.25
4	3.64	44.6	34.8	12.1
5	3.78	41.1	38.6	15.0
6	4.15	0	45.8	21.0

*Not actual volume ratios because of pressure in generator duct.

A maximum power output of 21 watts was obtained.

Since in this experiment the total resistance of the circuit is large compared to the shunt resistance of the external load, particularly at high gas flowrates, a higher output could have been achieved had the impedance of the external load and generator been matched. Experiments are planned to measure the resistance of the various gas-NaK mixtures common to these experiments.

C. Rocket Fuel Test Reactor (RFTR)

As part of a program to study and evaluate the application of nuclear reactors for thermal-rocket propulsion, the concept of using a reactor to test fractions of prototype cores under design conditions is being investigated. A test reactor should, therefore, in principle, consist of a center test section surrounded by a peripheral driver section. The test reactor concept should reduce testing costs, including a reduction in the quantity of hydrogen required for tests of long duration.

The minimum power density for some proposed rocket reactor cores is 10 Mw/liter. It is desired to test a fraction of the prototype core with a

volume as large as 20-30 liters. The total power of the driver should not exceed several hundred megawatts.

A parametric study of the two promising driver systems selected from earlier survey calculations are being investigated; namely, a BeO-UO_2-fueled, sodium-cooled epithermal system and a zirconium-uranium alloy-fueled, sodium-cooled fast system.

Parametric studies of the beryllium oxide and zirconium driver systems in finite cylinder geometry are about 80% completed. RE-122 diffusion theory calculations have been run for test sections having radii of 3, 6, 9, and 13 cm with various driver loadings. A synopsis of the results of test sections having a radius of 9 cm is given in Table XII. The two types of test sections used in the calculation are described below.

Table XII. Results of Driver Test Section Physics Calculations with 9-cm Test Sections

Test Section Series and Driver Type	Driver Loading % UO_2 or U	Critical Radius (cm)	Max Power Density Ratio	Test Section Max/Avg Radial Power Ratio
A-BeO	5	41.1	2.83	1.09
A-BeO	2.5	56.8	3.79	1.14
A-Zr	5	44.0	2.19	1.01
A-Zr	3	73.8	3.43	1.01
B-BeO	5	44.0	1.98	1.12
B-BeO	2.5	60.7	2.56	1.20
B-Zr	5	46.9	1.51	1.00
B-Zr	3	81.5	2.38	1.04

Two test section compositions have been studied; i.e., series A and B, and a third, series C, is in progress.

Test Section Volume Fraction/System	Series A	Series B	Series C
Void	0.44	0.35	0.40
UO_2	0.22	0.16	0.30
W	0.34	0.49	0.30

At this point, the zirconium system does not appear as attractive as the beryllium oxide system. The zirconium system requires roughly twice the total power as reflected by the larger critical radius to obtain the higher ratio of power density between the test section and the driver section.

D. Steel Industry Study

A study has been initiated to evaluate the application of nuclear energy to the steel industry. The study must consider direct nuclear energy application to be of value, since cheap electricity is already an objective of the U.S. reactor development program. It is planned to investigate some novel techniques which will make use of some of the unique aspects of nuclear energy.

V. NUCLEAR SAFETY

A. Thermal Reactor Safety Studies

1. Metal Oxidation and Ignition Studies

a. Ignition of Plutonium and Plutonium Alloys. Ignition studies of binary alloys of plutonium have been completed. The effects of 2 atom percent additions of carbon, aluminum, silicon, chromium, manganese, iron, cobalt, nickel, cerium, and uranium on the ignition temperatures of plutonium foils, when ignited in air or oxygen, have been appraised.

The ignition temperatures of pure plutonium fall within two regimes, one at about 500°C and the other at about 300°C. Whether the plutonium ignition temperature falls within the high-temperature (500°C) regime or whether it falls within the low-temperature (300°C) regime depends upon the specific area of the foil. In air, pure plutonium foils having specific areas less than 2 sq cm/g ignite at about 500°C; plutonium foils having specific areas greater than 2 sq cm/g ignite at about 300°C. In oxygen, the transition from the 500°C regime to the 300°C regime occurs at a specific area of about 6 sq cm/g.

The existence of two regimes of ignition is consistent with the oxidation behavior of plutonium. During the oxidation of plutonium two regimes are evident, one above 420°C and the other below 320°C. This behavior is ascribed to a change in the kinetics of the oxidation reaction which occurs between 320 and 420°C (see Progress Report for March 1963, ANL-6705, page 63).

The effects of additives on the behavior of plutonium in the high-temperature regime were as follows:

(1) Additives that increased resistance to ignition and oxidation: aluminum and silicon.

(2) Additives that had no effect: chromium, iron, nickel, cerium, and uranium.

(3) Additives that decreased resistance to ignition and oxidation: carbon, manganese, and cobalt.

The effects of additives on the behavior of plutonium in the low-temperature regime were as follows:

(1) Additives that increased resistance to ignition and oxidation: chromium and manganese.

(2) Additives that had no effect: silicon and nickel.

(3) Additives that decreased resistance to ignition and oxidation: iron and uranium.

Over the specific areas of foils studied (0.5 sq cm/g to 10 sq cm/g), no transition from the high-temperature regime to the low-temperature regime was observed for binary alloys of plutonium containing carbon, aluminum, cobalt, or cerium.

b. Aluminum-U_3O_8 Reaction. Studies of the aluminum-U_3O_8 thermite reaction were continued (see Progress Report for June 1963, ANL-6749, page 58). Cold-pressed compacts of aluminum-U_3O_8, containing 30, 45, 60, 75, and 90 w/o U_3O_8, were used. The samples were heated at a uniform rate of 25°C per minute to above 1300°C. Self-heating was noted with all samples except the one that contained 30 w/o U_3O_8. The most vigorous reaction occurred with the specimen that contained 60 w/o U_3O_8. With this sample, the temperature rose spontaneously to about 1300°C when the furnace temperature approached 900°C. The extent of reaction will be established by determining the amount of oxides remaining in the residue after reaction. A technique based on the selective dissolution of the metallic phases in an iodine-methanol solution has given promising results in preliminary tests.

B. Fast Reactor Safety Studies

Fast power reactor designs contain sufficient fuel to produce a superprompt critical assembly if the core were rearranged into a sufficiently compact mass. Hence, it is possible to postulate a class of "meltdown" incidents in which the core is subjected to abnormal operating conditions, some degree of fuel failure occurs, and the fuel moves into a more compact mass that results in a destructive burst of nuclear power. It is of interest to understand the detailed mechanisms involved in the rearrangements of fuel and, if possible, to develop designs which will eliminate the possibility of violent disassociation.

TREAT is being used to perform in-pile experiments to study the characteristics of failure in fast reactor fuel elements, and to survey the mechanisms influencing movement of fuel.

1. Summary of Dry Tests on Pre-irradiated Metallic Elements

A total of eleven experiments have been run in opaque dry meltdown capsules on previously irradiated samples. Seven were EBR-II, Mark I (5% fissium alloy) specimens which had been irradiated in the MTR at a calculated maximum centerline temperature of 445°C up to a maximum burnup of about 1 a/o. The remaining four were half-length Fermi Core-A elements, 10 w/o molybdenum-uranium pins clad with a 0.125-mm thick zirconium jacket by extrusion, which were irradiated at 460°C maximum centerline temperature to an estimated burnup of 0.25 a/o.

Results of the tests may be summarized in the form of a comparison with previous results on unirradiated elements:

EBR-II (Uranium-5% Fissium) Elements

(1) Irradiated and unirradiated pins start swelling at approximately the same excursion conditions.

(2) Amount of burnup does not have a great effect on threshold of failure for the ranges considered.

(3) The failure mechanism of very low burnup (~0.09 a/o) samples is essentially the same as that of unirradiated samples.

(4) The meltdown residue of moderate burnup (~1 a/o) samples has more numerous and larger voids, and has about half the density of the unirradiated elements.

Fermi A (Uranium-Molybdenum) Elements

(1) Unirradiated Fermi pins withstood bursts up to 34-37 Mw-sec total integrated power in TREAT without noticeable damage. Irradiated pins began to swell at 27 Mw-sec, and failed at the melting point (about 29 Mw-sec).

A study was made of the swelling of the four EBR-II elements subjected to the most severe transients (burnups ranging from 0.09 a/o to 0.9 a/o, in which the maximum cladding temperatures were estimated to be about 1000°C or above). It was found that the void volume in the meltdown remains could be calculated, within 20%, for these burnups by the empirical relation

$$V = 50\,B \quad ,$$

where V is the v/o void and B is the burnup in a/o.

2. In-pile Failure Time Measurements

Results were reported previously (ANL-6698, Progress Report for February, 1963, p. 65; and ANL-6717, Progress Report for April, 1963, p. 65) for measurements made in TREAT on the time of failure of stainless steel-clad pins of uranium and uranium-5 w/o fissium. However, the in-pile failure time data for the unbonded elements were erratic and indicated very short penetration times. This difference is explained as possibly resulting from excessive thermal stresses in the steel cladding caused by melting fuel slumping against the cladding and setting up large temperature

gradients. One photographic experiment was performed to substantiate this hypothesis. Two stainless steel-clad pins, one bonded and one unbonded, were placed in a transparent meltdown capsule and exposed to an excursion sufficient to melt the fuel. Early failure occurred in the unbonded sample. The photographic record clearly showed the molten fuel running out of localized flaws approximately 1 mm size in the cladding. Failure of the sodium-bonded element occurred later in agreement with the earlier post-mortem reconstructions.

VI. PUBLICATIONS

Papers

KINETICS OF HETEROGENEOUS ELECTRON TRANSFER IN ELECTRODE PROCESSES

N. R. Stalica and J. Jordan

Handbook of Analytical Chemistry, ed. L. Meites. McGraw-Hill Book Co., Inc., New York, 1963. pp. 38-46.

THE ENTHALPIES OF FORMATION OF ZIRCONIUM DIHYDRIDE AND ZIRCONIUM DIDEUTERIDE

D. R. Frederickson, R. L. Nuttall, H. E. Flotow, and W. N. Hubbard

J. Phys. Chem. 67, 1506-1509 (July 1963).

METALLURGICAL STUDIES OF THORIUM-URANIUM-PLUTONIUM ALLOYS

B. Blumenthal

Proceedings of the Thorium Fuel Cycle Symposium, Gatlinburg, Tennessee, Dec. 5-7, 1962, TID-7650, Book II, 543-552 (Issued July 1963).

A FILM COPYING TECHNIQUE FOR IMPROVING RADIOGRAPHIC CONTRAST

N. S. Beyer, Harold Berger, N. P. Lapinski, and I. R. Kraska

Nondestructive Testing 21, 230-234 (July-August 1963).

NEW FABRICATION PROCESSES FOR HIGH-QUALITY TUBING

N. H. Polakowsi and J. E. Flinn, Jr

Proc. Intern. Conf. on Research in Production Engineering. ASME, New York, 1963. pp. 406-410.

EBR-II PROJECT

L. J. Koch

Proc. 1962 Ann. Conf. Atomic Industrial Forum. Atomic Industrial Forum, Inc., New York, 1963. pp. 28-29.

ATOMIC ENERGY COMMITTEE REPORT

S. H. Fistedis, R. R. French, B. B. Ewing, T. R. Kroeschell, and E. A. Wimunc

Proc. Ill. Soc. Professional Engineers 78, 18-21. (May 3-4, 1963)

THERMAL SELF-SHIELDING AND EDGE EFFECTS IN ABSORBING FOILS

J. L. Crane and R. C. Doerner

Nucl. Sci. Eng. 16, 259-262 (July 1963).

AN EFFICIENT COMPOSITE FORMULA FOR MULTIDIMENSIONAL QUADRATURE
H. C. Thacher, Jr
Commun. Assoc. Computing Mach. 6, 356-357 (July 1963).

CERTIFICATION OF ALGORITHM 134 AND 158, EXPONENTIATION OF SERIES
H. C. Thacher, Jr
(Henry E. Fettis, Comm. ACM, October 1962)
Commun. Assoc. Computing Mach. 6, 390 (July 1963).

ANL Reports

ANL-6605 DESCRIPTION AND PROPOSED OPERATION OF THE FUEL CYCLE FACILITY FOR THE SECOND EXPERIMENTAL BREEDER REACTOR (EBR-II)
J. C. Hesson, M. J. Feldman, and L. Burris

ANL-6709 1559/RE: A CODE TO COMPUTE RESONANCE INTEGRALS IN MIXTURES
Charles N. Kelber

ANL-6713 CRITICAL STUDIES OF A SMALL URANIUM CARBIDE-FUELED REACTOR WITH A BERYLLIUM REFLECTOR (ZPR-III Assembly 40)
R. L. McVean, P. I. Amundson, G. S. Brunson, and J. M. Gasidlo

ANL-6716 TRANSFER FUNCTION SYNTHESIS AS A RATIO OF TWO COMPLEX POLYNOMIALS
C. K. Sanathanan and Judith Koerner